Version of Record: https://www.sciencedirect.com/science/article/pii/S0378383919302674
Manuscript_71e3258c2a0c1f2f29aaafef45f12cdb

Storm-Driven Erosion and Inundation of Barrier Islands from Dune- to Region-Scales

A Gharagozlou[a,*], JC Dietrich[a],
A Karanci[a], RA Luettich[b], MF Overton[a]

[a] *Dept. of Civil, Construction, and Environmental Engineering, NC State University, Campus Box 7908, 2501 Stinson Drive, 428 Mann Hall, Raleigh, NC 27695*
[b] *Institute of Marine Sciences, University of North Carolina, 150 Coker Hall, 3431 Arendell St, Morehead City, NC 28557*

Abstract

Barrier islands are susceptible to erosion, overwash, and breaching during intense storms. However, these processes are not represented typically in large-domain models for storm surge and coastal inundation. In this study, we explore the requirements for bridging the gap between dune-scale morphodynamic and region-scale flooding models. A high-resolution XBeach model is developed to represent the morphodynamics during Hurricane Isabel (2003) in the North Carolina (NC) Outer Banks. The model domain is extended to more than 30 km of Hatteras Island and is thus larger than in previous studies. The predicted dune erosion is in good agreement with post-storm observed topography, and an "excellent" Skill Score of 0.59 is obtained on this large domain. Sensitivity studies show the morphodynamic model accuracy is decreased as the mesh spacing is coarsened in the cross-shore direction, but the results are less sensitive to the alongshore resolution. A new metric to assess model skill, Water Overpassing Area (WOA), is introduced to account for the available flow pathway over the dune crest. Together, these findings allow for upscaled parameterizations of erosion in larger-domain models. The updated topography, obtained from XBeach prediction, is applied in a region-scale flooding model, thus allowing for enhanced flooding predictions in communities along the Outer Banks. It is found that, even using a fixed topography in region-scale model, the flooding predictions are improved significantly when post-storm topography from XBeach is implemented. These findings can be generalized to similar barrier island systems, which are common along the U.S. Gulf and Atlantic coasts.

Keywords: XBeach, Hurricane Isabel, Outer Banks, Coastal Morphodynamics, ADCIRC+SWAN

1. Introduction

Barrier islands are common coastal features and storm defenses. They line 10% of the world's open coasts, with 24% of the total within the U.S., including most of the Gulf and Atlantic coasts [1]. The coastline of North Carolina (NC) is characterized by barrier islands called the Outer Banks, which stretch 320 km,and

*Corresponding author
Email address: agharag@ncsu.edu (A Gharagozlou)

contain dunes with typical crest elevations of 3 to over 10.5 m [2]. They are highly vulnerable to erosion and flooding during tropical cyclones and winter storms [3], which occur frequently in NC [4].

Storm-driven surge and flooding have been studied in coastal NC, often via computational modeling on region-scales to include the barrier islands, lagoonal estuaries, and inner floodplains [5, 6]. For idealized storms in this system, the magnitude and extent of coastal inundation are sensitive to the storm's forward speed, size, and track angle relative to the coast [7, 8]. For perturbations of forecast storm tracks and intensities,accuracy can deteriorate significantly if the storm's track over the NC sounds and barrier islands is not predicted correctly [9]. For perturbations of storm forward speed and timing, the storm surge can interact nonlinearly with the tides, thus increasing and decreasing the total water levels in regions along the coastline of [10]. All of these storm effects can be represented in a high-resolution modeling system, which was automated to provide forecast guidance about coastal circulation and flooding [11, 12] and has been expanded for storms along the entire U.S. Gulf and Atlantic coast (e.g. `https://cera.coastalrisk.live`). However, while these studies considered the storm-driven waves and flooding near the barrier islands, they did not consider the erosion of beaches and dunes due to overwash and inundation.

Erosion and breaching of barrier islands during storms have an important role on nearshore hydrodynamics, and recent studies have explored these processes by using field and remotely-sensed data and numerical models. The Outer Banks vulnerabilities to inlet breaching have been identified at several locations [13, 14]. The opening and eventual closure of the breach at Pea Island due to Hurricane Irene has been characterized extensively with aerial photography and other remote sensing data [15, 16, 17, 18, 19]. Beach and dune erosion were modeled at cross-shore transects in the northern Outer Banks [20, 21], but the sediment transport was found to be dominant in the alongshore direction. These predictions were improved with newer models to include land cover effects on the dune erosion [22].

We emphasize the difference in scales between models for coastal flooding and erosion. Storm-driven waves and surge are modeled typically on region-scale domains to represent their interactions with the complex coastal landscape. Recent studies for coastal NC have applied models on unstructured meshes, which allow for computational resolution to vary from kilometers in open water, to hundreds of meters near the coastline and through the floodplains, and to tens of meters in the small-scale natural and man-made channels that convey surge into inland regions [23, 9]. Circulation and flooding are predicted at the Outer Banks with a minimum resolution of 50 to 200 m, thus limiting the representation of cross-shore beach profiles and alongshore dune crest variations. This resolution is typical of similar studies at global scale [24] or region scales (e.g. in U.S. [25, 26, 27], Australia [28], and Europe [29]).

In contrast, erosion of beaches, dunes, and inlets is modeled typically on smaller-scale domains. When breaches at Pea Island were predicted with a morphodynamic model, less than 1 km of coastline was considered with a minimum resolution of 1 to 2 m [30]. This resolution is typical of similar studies in other regions, e.g. Texas [31], Louisiana [32], and Florida [33, 34], although the domains have grown to now include 10 to 20 km of island coastline. While these models can predict accurately the erosion at specific locations,

their smaller-scale domains can limit their interactions with waves and flooding throughout the region.

These interactions may be significant. Erosion of beaches, dunes, and inlets will allow changes to circulation on the open coast and behind the island. It has been suggested that Isabel Inlet contributed much more to the local currents than the water levels [35], but that numerical study did not include waves, dune overwash, or morphodynamics. For the Chandeleur Islands in Louisiana, their removal could increase surge by 0.5 m near New Orleans [36] and wave heights by nearly 500 percent [37], while restored islands could delay the peak surge by 1 to 2 hr [37]This erosion may have affected significantly the flooding in the region. However, in these studies, the updated ground surface elevations were taken from remote-sensing data, and not from model predictions, and thus they could not consider the evolution of these interactions during the storms.

This study will explore these interactions via hindcast of Isabel's effects on Hatteras Island, specifically the dune erosion along a 30-km portion between the communities of Rodanthe and Avon. Our hypotheses are that: (a) in regions with relatively-uniform topography, a process-based morphodynamic model can be coarsened and expanded to a relatively-large domain, without sacrificing accuracy; and (b) the topographic elevation changes can be further upscaled and passed to region-scale models to allow overwash and inundation behind the dunes. This study will require a loose coupling of process-based modeling systems: the ADvanced CIRCulation (ADCIRC, [38, 39]) and Simulating WAves Nearshore (SWAN, [40, 41]) models, known as ADCIRC+SWAN, which have gained prominence for simulations of storm-driven waves and surge; and the eXtreme Beach (XBeach, [42]) model, which was developed explicitly for beach erosion during storms. Sensitivity tests will explore the relationship between accuracy and structured-mesh resolution in XBeach. Dune crest elevations will be passed to the unstructured mesh used by ADCIRC+SWAN, to allow for inundation of the communities on Hatteras Island and the results will be compared to XBeach prediction and the observations. This study is a necessary step toward the tight coupling of storm-driven erosion and flooding on region scales.

2. Hurricane Isabel (2003)

2.1. Synoptic History

Isabel was the most powerful storm during the 2003 Atlantic hurricane season, and its winds, waves, and storm surge impacted the NC Outer Banks. Isabel formed as a tropical wave off the West African coast on 1 September [43], strengthened into a tropical storm by 6 September, into a hurricane by 15:00 UTC 7 September, and became a Category-5 hurricane on the Saffir-Simpson scale by 18:00 UTC 11 September with maximum sustained winds estimated at 74 m/s. During the next week, the storm moved northwestward and weakened, becoming a Category-2 hurricane on 16 September with maximum wind speeds of 45 m/s (Figure 1). On 17:00 UTC 18 September, Isabel made landfall near Drum Inlet in the NC Outer Banks as a Category-2 hurricane. The storm continued to weaken as it moved across eastern NC and became a

tropical storm over southern Virginia. A day later, the storm weakened to extra-tropical and was eventually absorbed by a larger baroclinic system at 06:00 UTC 20 September [43].

Isabel produced significant wave heights of about 8.1 m at the USACE Field Research Facility in Duck, NC. This observation exceeded the previous 27-year record by 1.8 m [44]. Peak storm surge of 1.5 m occurred in phase with the time of high tide, which resulted in almost equal surge level along the northern Outer Banks and near the landfall location [45]. The National Oceanic and Atmospheric Administration (NOAA) water level gauge at the ocean-side of Cape Hatteras, recorded a water level of 2.05 m before failing during the storm [46]. A maximum water level of 1.45 m was recorded at the NOAA station at Oregon Inlet, NC, at 04:00 UTC 19 September, and 1.72 m at Duck station at 18:00 UTC 18 September. These waves and surge caused damages to infrastructure and permanent changes to the landscape.

2.2. Observed Erosion on Hatteras Island

Isabel caused erosion at several spots along the Outer Banks. The largest individual erosion event occurred near the western end of Hatteras Island, about 60 km east of Isabel's landfall location, where the island was breached due to extensive erosion, overwash, and flooding. The village of Hatteras was inaccessible due to the 520 m-wide inlet that connected the ocean and the sound. At this section, the island was narrowest with a width of about 150 m and the dune crest elevation was lower than other points along the island [45]. Elsewhere on the island, dunes were washed away at many locations, leaving sand deposits behind the dune, on the road, and against homes and other infrastructure. Dune erosion events occurred between the towns of Avon and Salvo. The town of Rodanthe was also impacted by a very large amount of erosion and overwash, causing damage to the buildings and road closure.

We select Isabel as a test case because of the extensive observations of morphodynamic changes to the topography of Hatteras Island. These changes are described in pre- and post-storm Light Detection and Ranging (LiDAR) surveys. Experimental Advanced Airborne Research LiDAR (EAARL) [47] surveys were conducted on 16 September (two days before landfall) and 21 September (three days after landfall), and cover a width of 200 to 400 m of the beach topography for a 350-km stretch of the Outer Banks [48]. The vertical and horizontal accuracy of these data are within 0.3 m and 1 m, respectively [49]. These high-resolution LiDAR surveys are especially valuable for understanding of the morphodynamic changes on the barrier island during the storm.

This barrier island is characterized by two parallel dunes, which are not completely continuous, and which merge into one dune in a few locations. The study area includes 30 km of Hatteras Island between the towns of Rodanthe and Avon (Figure 2). The peak, pre-storm, dune crest elevation is about 10 m relative to the North American Vertical Datum of 1988 (NAVD88), and the average dune crest elevation change due to the storm was about 1 m (Figure 3). Aerial photos from the EAARL surveys show more than 20 erosion events with widths of 100 to 300 m in this region. The extent of overwash fans from the shoreline varies between 80 to 200 m, where the sand deposits cover the road. Rodanthe was impacted by overwash and the northern side was covered by sand deposits with 5 km length and more than 200 m width.

3. Methods

3.1. Digital Elevation Model for Hatteras Island

The process-based, numerical models will require information about the pre-storm ground surface elevations as initial conditions, and about the post-storm ground elevations for validation. Thus, high-resolution digital elevation models (DEMs) were developed from existing sources. Bathymetric data were derived from a state-wide DEM with 10-m resolution that was developed for floodplain mapping studies [50]. This DEM was then supplemented with high-resolution pre-storm and post-storm LiDAR data for Hatteras Island topography [47]. To obtain high-resolution DEMs for the study area for both pre- and post-storm conditions, systematic errors were corrected in the raw LiDAR data [51]. Water turbidity, bubbles, and white foam in the surf zone can cause refraction of the laser beam that is emitted from survey equipment, so unreliable points in this region were removed from the dataset. The result point cloud covers 100 to 250 m width of the island. Each dataset was interpolated with the RST (Regularized Spline with Tension) method [52] into a 1-m raster. The bathymetry data and the LiDAR-based DEM may not align vertically on the edges of dataset, and thus a 30-m buffer zone was created to allow for a smooth linear transition between the LiDAR-based topography raster and the bathymetry DEM. The LiDAR point cloud is much denser on the dunes. Therefore, a uniform resolution of 1-m was selected to ensure efficiency and completeness of the raster. The resulting pre- and post-storm DEMs represent the ground surface elevations throughout the study area.

3.2. Large-Domain Models for Storm-Driven Waves and Circulation

3.2.1. Atmospheric Forcing

For storm simulations on large domains, atmospheric pressure and wind velocities are used as surface forcings for waves and circulation. This study uses a re-analysis product from OceanWeather Inc. based on land-, sea-, air-, and satellite-based observations [53]. For Isabel, the wind fields consist of surface pressures and wind velocities on a nested set of regular grids. The larger grid spans over 60° to 85° W longitude and 15° to 48° N latitude with a regular 0.125° resolution, and the nested sub-grid extends over 74° to 78° W longitude and 36° to 40° N latitude with a regular 0.025° resolution. Surface pressures and wind velocities are interpolated in time and space from these regular grids onto the unstructured mesh used by the hydrodynamic models.

3.2.2. ADCIRC+SWAN

The large-scale effects of Isabel on nearshore waves and circulation are predicted by using the tightly-coupled ADCIRC [38, 39] and SWAN [40] models, which are widely-used for storm surge and coastal flooding [53, 54, 9]. ADCIRC uses the continuous-Galerkin, finite-element method to solve modified forms of the shallow water equations on flexible, unstructured meshes. SWAN solves the wave action density equation for the evolution of wave energy, and it was extended to use unstructured meshes [41]. When coupled tightly, the ADCIRC+SWAN models can pass information through local memory without the need for

interpolation between models [55]. The coupled models can provide predictions of water levels, depth-averaged currents, and wave parameters (significant height, peak period, etc.) throughout a large domain, but with focused resolution in the coastal region of interest. ADCIRC+SWAN has been validated for coastal flooding applications along the U.S. Gulf (e.g., [26]) and Atlantic (e.g., [56]) coasts.

ADCIRC+SWAN predictions were saved at specific locations near Hatteras Island, and then used as boundary conditions for XBeach. Time series of ADCIRC water levels were saved at two locations offshore and two locations in the sound, and then used as boundary conditions at the four corners of the mesh used by the morphodynamic model (Figure 4). Time series of SWAN wave parameters (significant height, peak period, and mean direction) were saved at 15 locations at the offshore boundary in XBeach (Figure 4), which then uses the parameters to generate a JONSWAP spectrum with $\gamma = 3.3$ and directional spreading of 20, which is consistent with similar studies on the U.S. Atlantic [57] and Gulf coasts [34]. The morphodynamic model interpolates spatially and temporally the input boundary conditions to generate values along its boundaries.

3.2.3. Unstructured Mesh

This study uses an edited version of the high-resolution NC9 mesh (v9.98) [23], which has more than 90 percent of its mesh resolution in the NC coastal region (Figure 2). The resolution varies from 100 km in the Atlantic Ocean to 50 m in the nearshore of NC. The mesh extends inland to the 15-m topographic contour to allow for storm surge and flooding prediction. Ground elevations at the mesh vertices were interpolated from several high-resolution DEMs to resolve bathymetric and topographic features such as inlets, dunes and rivers [23].

The typical mesh resolution on Hatteras Island was about 100 m, and thus the beach and dune system was represented with only 1–2 elements in the cross-shore direction. To improve the representation of this system, the maximum resolution was increased to about 20 m on the Outer Banks between Cape Hatteras and Oregon Inlet. This resolution was selected partly due to concerns about model stability (i.e. to maintain an efficient time step under the Courant-Friedrichs-Lewy condition), but it was also informed by the XBeach mesh sensitivity results, as described in Section 4.3.

3.3. Process-Based Model for Morphodynamics

3.3.1. XBeach

XBeach [42], is a robust morphodynamic modeling tool for nearshore processes during extreme events. The model solves the time-varying, short-wave action balance equation and two-dimensional, depth-averaged shallow water equations of momentum and continuity and includes infragravity wave effect, avalanching, wave breaking, dissipation, etc.

For this study, several XBeach settings were calibrated differently from their defaults, but consistently with other recent studies. Table 1 describes these parameters and their associated values in this study. The time scale of bed level change is often much longer than for hydrodynamic processes, so XBeach uses an

acceleration scheme [58] to speed up the morphological evolution by a factor f_{mor} relative to the hydrodynamic time scale. Sensitivity tests have shown an improvement in computation time for f_{mor} up to 20 [32], while the difference in model results was less than 2 percent; this study used $f_{mor} = 10$. The model was calibrated using two parameters. One parameter, γ_{ua}, accounts for the effects of wave asymmetry and skewness, which can have a significant influence on the sediment transport rate during overwash in the surf zone [59]. Sensitivity tests have shown an optimal value of $\gamma_{ua} = 0.3$ [57], which was used in this study. The other parameter, $S_{\max}$, is the Shields parameter and limits the returning flow speed during overwash. It has been shown that XBeach overestimates the erosion of the dunes during overwash, and this limiting parameter is needed to control the flow speed [33, 31]. Similar to previous studies, the best results were achieved by using $S_{\max} = 0.8$. The `wetslp` parameter defines the threshold for the start of avalanching on wet nodes. The $h_{\min}$ parameter prevents very strong return flows in very shallow water conditions. The values for these parameters were calibrated within their default ranges.

3.3.2. Structured Meshes

XBeach is applied on a large domain with a total length of about 32 km. A high-resolution mesh was generated to represent the bathymetry and topography of the barrier island (Figure 2). The model incorporates this curvilinear mesh with 2100 × 420 cells with coverage of the island between the towns of Avon to Rodanthe. To allow for development of waves at the boundary, the mesh extends 2 km offshore and 1.8 km on the lagoon side. Mesh resolution varies locally in cross-shore direction with minimum of 3-m cell spacing on the beach and on the surf zone, and maximum of 30 m at the offshore boundary. Alongshore spacing of this mesh is about 15 m.

In addition to the large-domain mesh, smaller meshes with varying resolutions were generated to analyze the sensitivity of model accuracy. These smaller meshes cover a 4-km sub-region of the larger mesh, extend 2 km in offshore direction and 1.8km on the lagoon side (Figure 2). The sub-region coincides with the largest dune erosion of 3 m during Isabel. All XBeach parameters are consistent between region and sub-region, and boundary conditions were implemented from ADCIRC+SWAN simulation results. In the sub-region, a 'base' mesh was constructed to have a constant alongshore spacing of 15 m and minimum cross-shore spacing of 3 m (Table 4). Then in sensitivity studies, the mesh spacing in alongshore direction is increased up to 200 m and decreased down to 5 m, and the cross-shore mesh spacing is changed from 3 m to 30 m.

3.3.3. Representation of Dunes on Coarser Meshes

The dune system is an important topographic feature which acts as a hydraulic obstacle and prevents flooding into the lagoon. We used a method (see Appendix) to represent the dune crest in the models (XBeach and ADCIRC). This process informed a method to evaluate the dune crest elevation and is the basis for the Water Overpassing Area (WOA), a new metric developed for this study. The WOA is calculated along the dune crest line by integrating the vertical area above the dune crest and below a given elevation, e.g. the area between the dune crest and an elevation of 4 m. Thus it is an estimate of the available pathway

for flow over the dunes and into the back-barrier area. This metric can be calculated for a variety of dune crests, as represented at different scales in the DEMs and models, and for a variety of potential water levels, as represented by different elevations, and thus it can be used to evaluate the upscaling process. If the WOA matches between the source and target, the potential for water to overpass the dune crest is maintained. In this study, the WOA was used to assess the accuracy of upscaled dune crest lines in model inputs, to assess the accuracy of predicted dune crest erosion for a single XBeach simulation, and also to compare results between XBeach and ADCIRC.

3.4. Model Accuracy

XBeach model predictions are compared to pre- and post-storm observations, and the model accuracy is calculated with several metrics. These calculations are performed only on the region that contains the LiDAR survey data. We use three metrics: the water overpassing area WOA, the bias B_{MN}, the skill score SS.

Bias (B_{MN}) is the mean error between predictions and observations, and it is calculated as a point-to-point difference. A negative B_{MN} will indicate an overestimation of erosion, while a positive B_{MN} will indicate an underestimation in erosion. The B_{MN} is computed as:

$$B_{MN} = \frac{1}{N}\sum_{i=1}^{N}(z_{p,i} - z_{o,i}) \tag{1}$$

where N is the number of points (described later), z_p is the predicted topographic elevation (from XBeach), and z_o is the observed topographic elevation (from DEM).

Skill Score (SS) is a comparison of the error in predicted bed level change to the variance of observed bed level change. A SS value of unity indicates a perfect match between predictions and observations, and lesser values indicate a progressively worse match. The SS is computed as:

$$SS = 1 - \frac{\sum_{i=1}^{N}(\Delta z_{o,i} - \Delta z_{p,i})^2}{\sum_{i=1}^{N}(\Delta z_{o,i})^2} \tag{2}$$

where Δz_o is the change in observed elevation (between pre- and post-storm conditions), and Δz_p is the change in predicted elevation (again, between pre- and post-storm conditions).

For both B_{MN} and SS, we emphasize a difference between our method and previous studies [33, 31], which calculated SS at the XBeach mesh resolution, i.e. by comparing erosion predictions only at the computational points. However, our analyses will show that SS is sensitive to the resolution over which the calculation is performed. Therefore, we will compute B_{MN} and SS with two methods. (1) Similar to the previous studies, pre and post-storm DEMs are interpolated onto the XBeach mesh, and then B_{MN_1} and SS_1 are calculated over the XBeach mesh vertices. Thus, the number of points (N) depends on the the resolution of the mesh. (2) Model outputs are linearly interpolated into a 1-m DEM, and then SS_2 is calculated using this DEM and pre- and post-storm DEMs. In this method, the number of raster cells is constant for all 4-km meshes regardless of their resolution.

It is noted that, for the second method, the interpolation of XBeach results onto the 1-m DEM can add error to the B_{MN_2} and SS_2 calculations. To quantify the contribution of this interpolation error, we calculated an SS_2 value by examining only the observed topographic changes, without any XBeach simulation. The post-storm DEM was interpolated onto the base 4-km XBeach mesh and back onto the 1-m DEM, and then this double-interpolated DEM was used as the 'predicted' post-storm condition in an SS_2 calculation. If the interpolation did not introduce any errors, then this SS_2 value should be unity; instead, we found $SS_2 = 0.94$ for this case. It is noted that this interpolation error does contribute to the overall error, but it is relatively small compared to the SS_2 values computed from the XBeach predictions (Table 4), described in the following section.

4. Results and Discussion

The ADCIRC+SWAN predictions are validated for waves and water levels during Isabel. XBeach model performance is analyzed via comparisons with post-storm DEM and aerial imagery. Then, the sensitivity of XBeach to its mesh resolution is quantified by varying systematically the alongshore and cross-shore mesh spacings. Finally, the predicted topographic changes are upscaled for use in a repeated ADCIRC+SWAN prediction, but now representing the lower beach and dune elevations, and thus allowing more flooding into coastal communities.

4.1. Predictions of Storm Waves and Surge in Coastal NC

The SWAN predictions are a good match to observations at buoys ranging from deep water to the nearshore (Table 2, Figure 5). At NDBC buoys 41001 and 41002, which are located in deep water to the east and south of Cape Hatteras, respectively, the significant wave heights increase to peaks of about 10 m, although the records are missing data as the storm passed nearby. The SWAN predictions match the development of the largest significant wave heights at these locations.At NDBC buoy 41025 on the shelf at Diamond Shoals, close to the storm's landfall, the observations show a significant wave height of almost 14 m before the buoy failed. The SWAN predictions match the magnitude of this peak, but are delayed by 6 to 8 hr after the buoy failure. At buoys on the shelf but farther from the storm's landfall, such as the NDBC buoy 44056 at the USACE Field Research Facility near Duck and NDBC buoy 41013 at Frying Pan Shoals near Wilmington, the observed significant wave heights are smaller, with peaks of about 8 m and 6 m, respectively. The SWAN predictions show similar peaks, and they fill the gaps in the observed record during the storm.

Water levels were observed at NOAA tide gauges along the NC coast, and they show variations in the peak water levels (Figure 6). At gauges to the south of the storm's landfall, the observed peak water levels are not much larger than the tide range. At NOAA station 8658120 at Wilmington, there is no observed storm peak, while at NOAA station 8656483 at Beaufort, the observed peak water levels are about 1 m, and are matched within 0.1 m by the ADCIRC predictions. At gauges in the northern part of the coast near Oregon Inlet and

Duck, which are closest to our study area on Hatteras Island, the peak water levels were observed as large as 1.5 to 2 m. The ADCIRC predictions show the timing of these peaks, and they match their magnitudes within 0.1 to 0.25 m. Although the Oregon Inlet station is located on the sound side of the Outer Banks, the ADCIRC predictions match the observed water levels. On the ocean side, the predictions agree with the observations at the buoy and gauges, thus giving confidence in the ADCIRC+SWAN predictions. The accuracy of predicted significant wave heights and water levels at the stations near the study area is acceptable for the purposes of this study, and the extracted boundary conditions from ADCIRC+SWAN will be used for the XBeach simulations.

4.2. Erosion of Beach-Dune System on Hatteras Island

Model simulations can predict the timing and evolution of the erosion events, relative both to each other and to the incoming waves and surge during the storm. Furthermore, the extent and volume of erosion and deposition of sediments, and the growth pattern of the overwash fans relative to time-varying water levels, are investigated via analyses of the model predictions. Along the 30-km portion of the island, the beach and dune systems are in the swash regime at the start of the storm. Increasing wave height and water level initiate collision regime and the dune face gets eroded gradually. Inundation occurs in several locations where the dunes are lowered. To better understand and describe these morphodynamic changes, three locations that contain erosion events are selected (Figures 7a and 8a).

In the northernmost part of the domain near Rodanthe (Figures 7b-c), the water level starts to increase at 11:00 UTC 18 September, or 6 hr before landfall. About 6 hr later, the water levels reach their maxima, and the beach undergoes its maximum inundation. Relatively-low dune elevations, as well as dune and beach erosion (Figures 8b-c), lead to inundation at this region. XBeach predicts peak water levels that inundate much of the island. This is an overestimation; the aerial photos show evidence of overwash fans and inundation, but only in specific locations. However, extensive deposition of sand in this region implies relatively larger flooding, and it is noted that the predicted peak water depths are only about 10 cm over much of this region. Additionally, our XBeach implementation does not include effects of land cover and vegetated areas, which would likely limit the flooding area behind the dune system. Dune removal and inundation, followed by dune face erosion, are visible in the beach profiles as they evolve in the XBeach predictions (Figure 9a). By 17:00 UTC 18 September, the dune has been removed completely, and the peak ground elevation is within 0.5 m of the observed peak in the DEM. The volume of sub-aerial erosion between 11:00 and 21:00 UTC 18 September is $0.58 \cdot 10^5$ m^3, and, during this time, the maximum erosion rate of $5.9 \cdot 10^3$ m^3/hr has occurred at this section of the beach. Observations show more than 3 m of erosion on the beach, and sand was moved onto the road behind the dunes. Predicted erosion on the beach and dune is close to the observations. Although XBeach predicted the overwash fans behind the dunes, the extent and amount of sand deposition is underestimated. The total predicted deposition volume is 72 percent of the observed deposition.

Erosion and overwash were similar on the primary dune in the middle part of the domain, but the inundation was slowed by a secondary dune. The overwash started at 13:00 UTC 18 September or 4 hr before landfall, as the water crossed the primary dune. However, the secondary dune prevented flooding in the road and back-dune. The extent of overwash fans and flooding in this region were much smaller than in the northern region near Rodanthe, likely because the relatively higher dune crest acted to hinder the flooding (Figure 3). Maximum flooding coincided with the highest surge level at 17:00 UTC 18 September. In this portion of the island, the predicted overwash extent and the flooded wet areas in the aerial photos are represented well by the model. The erosion events and the extent of eroded dunes are also predicted accurately in XBeach (Figures 7d-e and 8d-e). In this region, the maximum erosion rate was $3.54 \cdot 10^3$ m^3/hr between 11:00 and 21:00 UTC 18 September, with a total dune and beach erosion of $1.11 \cdot 10^5$ m^3 ,which is close to observation ($1.21 \cdot 10^5$ m^3). But the amount of deposition on the road is not predicted accurately. The dunes in this region have generally higher elevation and are not removed completely, however, local erosion is predicted well. Figures 8d-e show the amount of erosion and deposition on the beach and behind the dune system. The maximum of 4 m dune crest elevation change occurred at this section where the dune is removed.

At the southern part of the domain, the overwash starts at 16:00 UTC 18 September or 1 hr before landfall. Similar to the middle section, high dunes (Figure 3) prevent flooding until the maximum surge reaches the coast. In this region, two parallel dunes protect the rest of the island from erosion and overwash. In Figures 7f-g, the primary dune has eroded, but the secondary dune has blocked and trapped the flood waters between the dunes. The accuracy of XBeach in predicting the locations of the erosion events and overwash fans in this region is encouraging. Figure 7 shows the extents of maximum flooding during the simulation at different locations on the beach. A qualitative comparison of these results and post-storm aerial photos confirms that XBeach captured these events. The extents of erosion and deposition at the southern region is provided in Figure 8f, and comparison to Figure 8g confirms that the predictions are very close to observations. The total amount of deposited sediment behind the dunes is underestimated in XBeach by 15% (Figure 8 and Table 3). The volume of erosion computed from observed DEMs ($0.94 \cdot 10^5$ m^3) is close to the prediction ($0.88 \cdot 10^5$ m^3).

The predicted erosion and deposition are compared to observations of topographic elevation changes (Figure 8), and the corresponding volume of sediment transported is calculated over the extents of available LiDAR observations (Table 3) and also the rate of erosion and deposition for each region is computed over time (Figure 10). As the waves and water levels increase, the erosion rate also increases. The maximum rate of sediment transport occurs between 11:00 and 21:00 UTC 18 September during the overwash and inundation regimes. Figure 9 shows the beach profile evolution at several time steps. The evolution of the profile is in agreement with the regimes that occur on the beach. The erosion on the dune face happens during the collision regime, and, after 11:00 UTC 18 September as the water levels and wave heights increase, the overwash and inundation regimes start and sediment transport reaches its maximum rate. After 02:00

UTC 19 September, with water levels receding and the wave heights decreasing, the erosion slows down and deposition rate goes to zero. The final profile matches the post-storm DEM, and the shape of the dune is predicted well in cases that the dune is eroded partially or removed entirely.

The accuracy of morphodynamics predictions can be quantified via the SS_1 and B_{MN} metrics, which were computed for topographic elevation changes in more than 92,000 model cells. For the overall study domain, the $B_{MN} = 0.03$ m and $SS_1 = 0.59$, which can be categorized as 'Excellent' [60, 61]. When the observed and predicted elevation changes are compared (Figure 11), areas of high observed erosion are slightly under predicted by the model, however, most changes are near the 1-to-1 line. The good agreement between predicted and DEM-observed elevation changes can also be seen in the final XBeach profiles and the post-storm conditions. In most regions, XBeach represents well the dune erosion and removal. These predictions are promising for implementation of XBeach for morphodynamics on larger domains. In this large-domain modeling approach, the general behavior of the beach and dune erosion is more important than small-scale changes, and we will use the response of the beach to improve the flood prediction in larger-domain models.

Dunes are the primary hydraulic barriers to prevent flooding from extending over the island. Thus, predictions of the dune crest elevation change will be critical for coupling to larger-domain flooding models. To quantify the accuracy of XBeach predictions of dune crest elevation change, the WOA parameter is used to estimate the pathway for water to overpass the dune. As mentioned in 3.3.3, WOA uses the dune crest shape and the water level to calculate the available area for the overpassing flow. In large-scale models like ADCIRC, the mesh resolution is coarser than what is needed to capture the shape of the dunes. WOA provides the required information for mapping the hydraulic barrier elevation from XBeach to ADCIRC. Additionally, it is a useful error metric for comparing the accuracy of predicted and observed dune crest elevation. The result analysis indicates that prediction of post-storm WOA is close to observed condition (Figure 12a). For water levels of up to 1.5 m, predicted WOA is zero. This means that the dune crest elevation is high enough to block the water below this level. The predicted WOA, however, starts to increase gradually as the water level exceeds 1.5 m and reaches $28 \cdot 10^3$ m^2 for water level of 6 m. The predicted WOA is very close to post-storm plot (Figure 12a) and the error is less than 10 percent for water levels above 4 m. To identify the source of this error, WOA was computed for every 5-km sub-sections in the domain. The analysis shows that the prediction of dune crest elevation is very good for the southern-half of the domain and there are some inaccuracies in the northern part where the town of Rodanthe is located.

4.3. Sensitivity of Erosion Predictions to Mesh Resolution

The XBeach simulations in the previous section are critical steps toward predictions of storm-driven morphodynamics on large domains. However, for these predictions to be useful during real-time forecasting, they will need to be expanded to even larger domains (such as the entire 80-km of Hatteras Island) and then be coupled to models for storm surge and overland flooding (such as ADCIRC+SWAN). For both of these goals, it may be necessary to coarsen the XBeach mesh resolution to improve its computational efficiency.

In this section, we explore the sensitivity of the XBeach prediction accuracy to changes in mesh resolution, by varying systematically the along-shore and cross-shore mesh spacings in a section of Hatteras Island.

Instead of using the full XBeach domain from the previous section, the resolution sensitivity tests were run on a smaller domain (described in Section 3.3.2). This mesh covers a sub-region that includes processes such as local dune removal and flooding, and the variation in dune shape and height can be representative of the larger domain. The 4-km base mesh was initialized with the same resolution as the larger 30-km domain mesh; the resolution has a minimum of 3 m in the cross-shore and a constant 15 m in the alongshore directions. The base mesh has coverage of a major erosion event where the washover sedimentation blocked the NC 12 Highway. On this smaller domain, the XBeach predictions were validated with the $B_{MN} = -0.06$ m and $SS_1 = 0.68$, which can be categorized as 'Excellent' [61, 60]. In addition, the predicted dune crest shape and WOA are a good match to the post-storm profile (Figure 12).

This small-domain model was then used to investigate the effects of mesh resolution variation on accuracy. The alongshore and cross-shore mesh spacings were varied separately, by developing suites of meshes (Table 4). For each new mesh, the WOA metric and the additional pre-processing step (Section 3.3.3) were used to ensure that the pre-storm topographic condition as the initial setup in XBeach was similar for all meshes. Therefore, the differences in the XBeach predictions for each mesh are only influenced by mesh resolution.

For a range of alongshore mesh resolutions (Table 4), if SS is calculated at the mesh resolution, then it is not sensitive to alongshore spacing. The SS_1 values are relatively constant between $SS_1 = 0.67$ and $SS_1 = 0.69$ even for alongshore spacings up to 200 m, thus indicating that XBeach is predicting well the erosion at its mesh nodes. However, when the erosion predictions are evaluated on the higher-resolution 1-m raster, and thus closer to the resolution of the observed topography, the SS_2 values are decreased as the mesh spacing is coarsened. From an 'Excellent' value of $SS_2 = 0.72$ for an alongshore spacing of 5 m, the predictions are decreased to a 'Good' value of $SS_2 = 0.44$ for an alongshore spacing of 200 m. The largest dropoff in accuracy occurs at alongshore spacings of about 50 m. These findings quantify the relationship between XBeach mesh resolution and predictive accuracy, and they provide an upper limit on alongshore mesh resolution for use in future models.

The WOA metric (Figure 12) also can vary as the resolution changes. For an alongshore mesh spacing of 5 m, the WOA is very close to the post-storm condition, and as the spacing increases to 100 m, the graph slightly deviates from post-storm and shows less WOA. This trend indicates that the dune crest is eroded less with the larger alongshore spacing, and thus there is less WOA to allow overwash and inundation. However, the $L200$ mesh does not follow the same pattern, and its higher WOA is a good match to the post-storm conditions. When the WOA for the $L200$ mesh is considered alongside the $SS_2 = 0.44$ in Table 4, it is clear that this mesh resolution is insufficient to represent the erosion elsewhere in the beach and dune system. The WOA analysis of dune crest shape reveals the difference between each mesh resolution, where the dune crest in finer meshes is very close to post-storm. Even for an alongshore mesh spacing of 100 m, the predicted crest line is a good representation of the larger-scale high and low points on the crest.

These results suggest that very coarse meshes with alongshore spacing of more than 50 m are not ideal for capturing the morphology and dune crest erosion. Although individual values of SS and WOA may seem to be acceptable, their combined usage can reveal inaccuracies in the results. It is critical to examine the accuracy of the erosion predictions for both the dune crest and the entire beach and dune system, at the same resolution as the observations.

The XBeach model accuracy is more sensitive to mesh resolution in the cross-shore direction (Table 4). The SS_1 and SS_2 values both decrease as mesh spacings are coarsened, and they drop to almost 0 for the $C30$ mesh. The prediction of WOA also diverges from post-storm observations (Figure 12) as the mesh is coarsened. For the $Base$ and $C5$ meshes, the WOA shows that XBeach predicts the dune crests to be eroded close to the post-storm observations, whereas for the $C30$ mesh, the WOA shows no difference between the post-storm predictions and pre-storm observations. To better illustrate the effect of cross-shore mesh spacing on the predicted dune crest, modeled cross-shore beach profiles for each mesh are depicted in Figure 13. It can be seen that the dune erosion is not modeled correctly in coarser meshes, which fail to predict the removal of the primary dune. However, in the finer meshes, the first dune removal is predicted, and erosion is also seen at the second, higher secondary dune.

Interpolation and coarse representation of topographic features, in both the alongshore and cross-shore directions, can contribute to decay in predictive accuracy. The beach and dune erosion must be represented with sufficient resolution for XBeach. Otherwise, the model physics are impacted and consequently alter the results. For example in the $C30$ mesh, the beach and dune are represented with only 3 vertices, and thus the model cannot predict the erosion. For the alongshore variability, the decrease in WOA for the $L5$ to $L200$ meshes is less than what we observe in cross-shore resolution sensitivity. The dune crest elevation does not vary rapidly along the island, and thus the WOA has smaller changes as the alongshore mesh resolution is coarsened.

Coarsening the mesh will change the slope of the beach and dunes that are represented in the mesh and consequently hinder the avalanching and erosion. In order to investigate the effects of slope and to find the optimal performance for each mesh, the `wetslp` parameter is changed for each mesh separately. It should be noted that the impact of this parameter is more significant when the mesh spacing is changed in cross-shore direction. Calibrating the `wetslp` parameter for each mesh (Table 5) improved SS_1, and even for a very coarse $C30$ mesh we obtained $SS_1 = 0.92$. However, SS_2 decreases for higher cross-shore spacing (similar to the pattern observed when we used a constant `wetslp` for all meshes), and the WOA plots (Figure 14) for these tests show that the modeled dune crest is significantly lower for coarser meshes than the observed dune crest. Thus, calibrating with `wetslp` can improve accuracy in SS_1, but the other metrics show the model performance is still sensitive to the mesh resolution. We expect these findings to be similar for other storms in other coastal regions.

Thus, the XBeach predictions are sensitive to its alongshore and cross-shore mesh spacings, with significant changes in accuracy as represented by SS and WOA. The trends in SS depend on the resolution

at which this metric is calculated. While SS_1 is in 'Excellent' range for alongshore-coarsened meshes, SS_2 drops to 0.44 for the $L200$ mesh. However, the SS is more sensitive to cross-shore spacing, and both SS_1 and SS_2 decrease to zero for the $C30$ mesh. The erosion predictions deviate from post-storm conditions with coarsened resolution. These findings can provide guidance for the development of meshes to optimize accuracy and efficiency. Additionally, understanding the impacts of mesh resolution is the preliminary step toward upscaling the XBeach results to large-domain flooding models like ADCIRC.

4.4. Upscaling Eroded Topography to Larger-Domain Wave and Surge Models

Lastly, XBeach outputs are used to update the topographic features in ADCIRC+SWAN and to investigate the improvement of flooding predictions in region-scale models. We examine ADCIRC+SWAN simulations in which the island topography has been represented in three cases: (1) from a pre-storm DEM, (2) from a post-storm DEM, and (3) from the post-storm XBeach predictions.

Using the findings on mesh resolution in Section 4.3, the operational ADCIRC+SWAN mesh was refined in our study area on the Outer Banks. This refined mesh has a minimum resolution of 20 m on the study area, which is finer than its original resolution of $50 - 100$ m but is still coarser than the minimum cell size of 15×3 m in the XBeach mesh. In Cases 1 and 2, pre- and post-storm DEMs are interpolated onto the ADCIRC mesh. And in Case 3, the XBeach-predicted post-storm topography is used to update the island in the ADCIRC mesh. Then the large-scale model is run on each mesh to hindcast Hurricane Isabel, and the results are compared. To better focus the discussion, we analyze three regions, that include differences in the results of each Case (Figure 15); a section near Rodanthe, a section near the middle, and a section at the south part of the study area with discrete erosion events.

Near Rodanthe, ADCIRC+SWAN simulations for Cases 1 and 2 illustrate how the updated topography can impact the flooding prediction. The largest difference in flooding occurred at the northern part of the study area. Figures 15b-d show the maximum water elevation near Rodanthe, where extensive erosion allowed for dune removal and overwash from ocean to lagoon. In Case 1 with the pre-storm observed topography, the surge is pushed onto some parts on the beach, but the static dunes protect the back-barrier region and no flooding is observed on the island. However, in Case 2 with the post-storm observed topography, the dunes are fully eroded and flooding has occurred in this region. In the town of Rodanthe, the ocean and the lagoon are connected due to flooding (Figure 15c). This prediction was also observed earlier in XBeach (Figure 7b) as well as in post-storm aerial photos (Figure 7c). The results indicate that flood prediction can be improved considerably by integrating the topographic changes due to erosion in the model. In Case 3, the flooded area has even larger extents compared to Case 2 and it has a better match to flooding extent predicted in XBeach (Figure 15c). When the dune erosion and low-lying topography are updated from the XBeach results into the ADCIRC predictions, then there is a good match between the flooding predictions.

The models also provide information about how the flooding evolved during the storm. We consider transects at each of the three regions (with locations in Figure 15 and results in Figure 16a-b). At 11:00 UTC Sep 18, the ADCIRC water level exceeds 1 m on the ocean side of the island and initiates the flooding.

At 17:00 UTC Sep 18, the water level reaches its maxima of 2.1 m and subsequently the flooding extent grows. At the same time on the lagoon side, the wind pushes the water away from the island. The water level gradient between the ocean and the sound lets the water flow into the lagoon. The water level predicted by ADCIRC is discontinued near the shoreline because its mesh resolution does not allow the water line to extend to the true beach profile. Comparing the profiles at the northern section shows than the sand dune in Case 1 blocks the water flow ,however, in Case 3, the elevation of the dune is low enough to let the maximum surge at 17:00 UTC Sep 18 overtop the crest and flood the island. This result is very promising, and ADCIRC has shown a significant improvement in flood prediction with updated topography.

In the southern and middle sections with discrete erosion events, ADCIRC does not allow the overland flooding, even with the updated topography on the beach and dune system. In the middle section, ADCIRC predictions for Cases 1, 2 and 3 are very similar (Figure 15e-g), while the observation and XBeach prediction shows local flooding at this locations. Even in Case 3, ADCIRC could not capture the flooding in this region and the dunes prevented the flooding. The cross-section profiles (Figure 16c-d) show that the maximum water level exceeds 2.1 m at the coast, but the flooding is limited to the beach, and the water does not flow past the lowered dunes. ADCIRC does not represent the extra wave runup on the beach, and therefore the water level on the beach is slightly lower and water cannot cross the island. In the southern section, the dune is not fully eroded and is able to prevent flooding (Figure 16e-f) . These findings are encouraging, but more work is needed to upscale accurately the overwash and erosion processes to the region-scale models.

5. Conclusions

In this study, we explored the coupling of storm-driven erosion on beach and dune scales, with storm waves and flooding on region scales. ADCIRC+SWAN and XBeach models were developed for the impacts of Hurricane Isabel (2003) on Hatteras Island. Time series of offshore waves and water levels were predicted by ADCIRC+SWAN, and then used as boundary conditions for simulations of morphodynamics by XBeach. Overwash and inundation predictions were validated on a portion of the island including the towns of Rodanthe, Salvo, and Avon, and then the sensitivity of the erosion predictions was explored relative to the XBeach mesh resolution. Lastly, island topography in the ADCIRC mesh was updated by using the XBeach predictions. The major findings of this study are:

1. *XBeach was extended for predictions on a* 30*-km-wide domain, larger than any previous study.* Using default model settings and high-resolution pre-storm topography, we developed and validated an extensive model for storm-driven overwash and inundation. The accuracy with $SS = 0.59$ is in the 'Excellent' range [60]. There is a good match between the predicted inundation extents and erosion events to the post-storm observation, and the general behavior of dunes during various stages of the storm was modeled correctly.
2. *The Skill Score SS metric is sensitive to the mesh resolution.* This metric is used widely to assess the performance of morphodynamic models including XBeach, but it has considered differences between

observations and predictions only at the computational points. In our sensitivity study, we showed that SS should be computed at the same resolution as the observations.

3. *The XBeach accuracy is highly sensitive to its mesh resolution.* In the alongshore direction, the relatively-uniform dune crest along Hatteras Island allows for larger mesh spacings, and we did not see a decrease in model accuracy until the mesh was coarsened to an alongshore spacing of 50 m or larger. However, in the cross-shore direction, the accuracy was decreased significantly for mesh spacings larger than 5 to 10 m. These findings will have implications both for future studies with XBeach, as well as for coupling of XBeach predictions with other models.
4. *Even using a fixed topography in ADCIRC+SWAN, the flooding predictions are improved significantly when using post-storm topography from XBeach.* The differences in model prediction for each case are proof that accounting for morphodynamics in large-scale flooding models is critical. In island sections with extensive overwash, the updated topography can allow predictions of flooding across the island and through the coastal communities. However, more work is needed to represent the flooding allowed by discrete erosion events in the region-scale models.

These results are encouraging, especially given the relative simplicity of this XBeach model setup without vegetation or variability in sediments and other physical properties (i.e. bed friction, sand size, etc.). This level of simplification allows for transition of our findings to other regions. These finding may be specific to this region, however, the methodology can be applied in similar studies in other regions. Using a coarser mesh can improve the computational time, however, the SS_2 shows a significant reduction. Additionally, the prediction of the dune crest and WOA is very sensitive to the cross-shore resolution. Therefore, the optimal resolution depends on the purpose of the modeling and the accuracy and efficiency metrics that are of more interest and future testings will be necessary in other regions.

In this large-scale modeling approach, focus is on the general behavior of the beach and dune erosion, rather than small-scale changes. These findings will be used to provide a method for updating the topographic data in large-scale models based on the morphodynamic model results. This is a preliminary step toward two-way coupling of region-scale coastal flooding models such as ADCIRC and morphodynamic model such as XBeach. We explored the resolution requirements in each model, and the next goal is to find an optimal way of updating the topography, which may include correction or calibration of topographic data in order to accurately model the flooding. The findings of this study, including the morphodynamics of the beach and resolution requirements, can be used for bridging the gap between region-scale and dune-scale models and, therefore, improving the flooding predictions during storms.

Acknowledgements

The authors thank Dr. Helena Mitasova for her continuous help and support. This work was made possible by grants from the National Oceanic and Atmospheric Administration through the North Carolina

Sea Grant, and from the U.S. Army Corps of Engineers through the U.S. Coastal Research Program. This material is also based upon work supported by the National Science Foundation under Grant Award Number ICER-1664037, and by the U.S. Department of Homeland Security under Grant Award Number 2015-ST-061-ND0001-01. The views and conclusions contained in this document are those of the authors and should not be interpreted as necessarily representing the official policies, either expressed or implied, of the U.S. Department of Homeland Security.

Appendix: Mapping the Dune Crest on the Mesh

To represent the dune crest line in our models (XBeach and ADCIRC), the dune crest elevations were assigned in an extra step after interpolation of topographic data on to the mesh. For all of the meshes in our study, the ground surface elevations at all computational points were interpolated (upscaled) from fine-scale sources to a coarse-scale target. The source could be either a pre-storm DEM, post-storm DEM, or XBeach model result, while the target could be either XBeach or ADCIRC meshes. Interpolating the data with IDW or cell-area averaging method can cause smoothing of the dune crest elevations, which are then too low in the initial model topography. To preserve the dune crest in the model, we implement an additional post-interpolation process to correct the dune crest on the mesh. First, for each row in the DEM (perpendicular to the shoreline), we find the cells with the highest elevation (shown as white squares in Figure 17b). Then, for each row in the XBeach mesh (again, perpendicular to the shoreline), we find the vertices with the highest elevations assigned from the interpolation (shown as dark-red dots in Figure 17c). Finally, the elevations from the nearest DEM cells are averaged onto each of the dune-crest vertices (Figure 17d). This method has the benefit of maintaining the dune crest as a hydraulic obstacle to flow over the dune and island, while still being fully automated.

References

[1] M. L. Stutz, O. H. Pilkey, Open-ocean barrier islands: Global influence of climatic, oceanographic, and depositional settings, Journal of Coastal Research 27 (2011) 207–222 (2011).

[2] E. J. Sciaudone, L. Velasquez-Montoya, E. A. Smyre, M. F. Overton, Spatial and temporal variability in dune field: Pea island, north carolina, Shore and Beach 84 (2016) 49–58 (2016).

[3] K. S. Doran, H. F. Stockdon, K. L. Sopkin, D. M. Thompson, N. G. Plant, National assessment of hurricane-induced coastal erosion hazards: Mid-Atlantic Coast, Tech. Rep. 2013-1131, U.S. Geological Survey (2013).

[4] State Climate Office of North Carolina, http://climate.ncsu.edu/climate/hurricanes/statistics, [Retrieved 21 June 2017] (2017).

[5] R. J. Weaver, R. A. Luettich, 2D vs 3D storm surge sensitivity in ADCIRC: Case study of Hurricane Isabel, in: Estuarine and Coastal Modeling 2009, 2010, pp. 762–779 (2010).

[6] Y. P. Sheng, V. Alymov, V. A. Paramygin, Simulation of storm surge, wave, currents, and inundation in the Outer Banks and Chesapeake Bay during Hurricane Isabel in 2003: The importance of waves, Journal of Geophysical Research 115 (2010) C04008 (2010).

[7] M. Peng, L. Xie, L. J. Pietrafesa, A numerical study of storm surge and inundation in the Croatan-Albemarle-Pamlico estuary system, Estuarine, Coastal and Shelf Science 59 (2004) 121–137 (2004).

[8] M. Peng, L. Xie, L. J. Pietrafesa, Tropical cyclone induced asymmetry of sea level surge and fall and its presentation in a storm surge model with parametric wind fields, Ocean Modelling 14 (2006) 81–101 (2006).

[9] R. Cyriac, J. C. Dietrich, J. G. Fleming, B. O. Blanton, C. Kaiser, C. N. Dawson, R. A. Luettich, Variability in coastal flooding predictions due to forecast errors during Hurricane Arthur (2014), Coastal Engineering 137 (2018) 59–78 (2018).

[10] A. Thomas, J. C. Dietrich, T. G. Asher, B. O. Blanton, A. T. Cox, C. N. Dawson, J. G. Fleming, R. A. Luettich, Influence of storm timing and forward speed on tide-surge interactions during Hurricane Matthew, Ocean ModellingIn preparation (2018).

[11] C. Mattocks, C. Forbes, A real-time, event-triggered storm surge forecasting system for the state of North Carolina, Ocean Modelling 25 (2008) 95–119 (2008).

[12] B. O. Blanton, J. McGee, J. G. Fleming, C. Kaiser, H. Kaiser, H. Lander, R. A. Luettich, K. M. Dresback, R. L. Kolar, Urgent computing of storm surge for North Carolina's coast, in: Proceedings of the International Conference on Computational Science, Vol. 9, 2012, pp. 1677–1686 (2012).

[13] M. F. Overton, J. S. Fisher, Hurricane Isabel and the NC12 hotspots, Shore and Beach 72 (2004) 30–35 (2004).

[14] D. J. Mallinson, C. W. Smith, S. J. Culver, S. R. Riggs, D. Ames, Geological characteristics and spatial distribution of paleo-inlet channels beneath the outer banks barrier islands, North Carolina, USA, Estuarine, Coastal and Shelf Science 88 (2010) 175–189 (2010).

[15] A. S. Clinch, E. R. Russ, R. C. Oliver, H. Mitasova, M. F. Overton, Hurricane Irene and the Pea Island Breach: Pre-storm characterization and storm surge estimation using geospatial technologies, Shore and Beach 80 (2012) 1–10 (2012).

[16] E. J. Hardin, A transient landscape: Geospatial analysis and numerical modeling of coastal geomorphology in the Outer Banks, North Carolina, Ph.D. thesis, North Carolina State University (2013).

[17] M. F. Overton, E. A. Smyre, Evolution of the Pea Island Breach, Outer Banks, North Carolina, Shore and Beach 81 (2013) 23–27 (2013).

[18] L. Velasquez-Montoya, E. J. Sciaudone, H. Mitasova, M. F. Overton, Observation and modeling of the evolution of an ephemeral storm-induced inlet: Pea Island Breach, North Carolina, USA, Continental Shelf Research 156 (2018) 55–69 (2018).

[19] I. Safak, J. C. Warner, J. H. List, Barrier island breach evolution: Alongshore transport and bay-ocean pressure gradient interactions, Journal of Geophysical Research: Oceans 121 (2016) 8720–8730 (2016).

[20] L. A. Fauver, Toward predicting barrier island vulnerability: Simple models for dune erosion, Master's thesis, University of South Florida (2005).

[21] R. Gencarelli, G. R. Tomasicchio, N. Kobayashi, B. D. Johnson, Beach profile evolution and dune erosion due to the impact of Hurricane Isabel, in: International Conference on Coastal Engineering, 2009, pp. 1697–1709 (2009).

[22] A. Karanci, M. O. Kurum, M. F. Overton, Land cover effect on dune erosion and overwash, in: International Conference on Coastal Engineering, 2014 (2014).

[23] B. O. Blanton, R. A. Luettich, North Carolina Coastal Flood Analysis System: Model Grid Generation, Tech. Rep. TR-08-05, Renaissance Computing Institute (2008).

[24] S. Muis, M. Verlaan, H. C. Winsemius, J. C. J. H. Aerts, P. J. Ward, A global reanalysis of storm surges and extreme sea levels, Nat. Commun. 7 (11969) (2016).

[25] A. B. Kennedy, U. Gravois, B. C. Zachry, J. J. Westerink, M. E. Hope, J. C. Dietrich, M. D. Powell, A. T. Cox, R. A. Luettich, R. G. Dean, Origin of the Hurricane Ike forerunner surge, Geophysical Research Letters 38(8) (2011).

[26] J. C. Dietrich, A. Muhammad, M. Curcic, A. Fathi, C. N. Dawson, S. S. Chen, R. A. Luettich, Sensitivity of storm surge predictions to atmospheric forcing during Hurricane Isaac, Journal of Waterway, Port, Coastal and Ocean Engineering 144 (2018).

[27] M. V. Bilskie, S. C. Hagen, S. C. Medeiros, A. T. Cox, M. Salisbury, D. Coggin, Data and numerical analysis of astronomic tides, wind–waves, and hurricane storm surge along the Northern Gulf of Mexico, Journal of Geophysical Research: Oceans 121 (5) (2016) 3625–3658 (2016).

[28] I. D. Haigh, E. M. S. Wijeratne, L. R. MacPherson, C. B. Pattiaratchi, M. S. Mason, R. P. Crompton, S. George, Estimating present day extreme water level exceedance probabilities around the coastline of australia: tides, extra-tropical storm surges and mean sea level, Climate Dynamics 42 (2014) 121–138 (2014).

[29] T. Fernandez-Montblanc, M. I. Vousdoukas, P. Ciavola, E. Voukouvalas, L. Mentaschi, G. Breyiannis, L. Feyen, P. Salamon, Towards robust pan-european storm surge forecasting, Ocean Modelling 133 (2019) 129–144 (2019).

[30] M. O. Kurum, M. F. Overton, Scenario testing on the impact of topography, land cover and sea-level rise on barrier island breaching, in: Proceedings of Coastal Dynamics 2013, 2013, pp. 1025–1036 (2013).

[31] C. Harter, J. Figlus, Numerical modeling of the morphodynamic response of a low-lying barrier island beach and foredune system inundated during hurricane ike using xbeach and cshore, Coastal Engineering 120 (2017) 64–74 (2017).

[32] C. A. Lindemer, N. G. Plant, J. A. Puleo, D. M. Thompson, T. V. Wamsley, Numerical simulation of a low-lying barrier island's morphological response to Hurricane Katrina, Coastal Engineering 57 (2010) 995–995 (2010).

[33] R. T. McCall, J. S. M. van Thiel de Vries, N. G. Plant, A. R. van Dongeren, J. A. Roelvink, D. M. Thompson, A. J. H. M. Reniers, Two-dimensional time dependent hurricane overwash and erosion modeling at Santa Rosa Island, Coastal Engineering 57 (2010) 668–683 (2010).

[34] D. L. Passeri, J. W. Long, N. G. Plant, M. V. Bilskie, S. C. Hagen, The influence of bed friction variability due to land cover on storm-driven barrier island morphodynamics, Coastal Engineering 132 (2018) 82–94 (2018).

[35] M. O. Kurum, B. L. Edge, H. Mitasova, M. F. Overton, Effects of coastal landform changes on storm surge along the Hatteras Island breach area, in: Proceedings of Coastal Engineering 2010, 2010, pp. 1–8 (2010).

[36] T. V. Wamsley, M. A. Cialone, J. M. Smith, B. A. Ebersole, A. S. Grzegorzewski, Influence of landscape restoration and degradation on storm surge and waves in southern Louisiana, Journal of Natural Hazards 51 (2009) 207–224 (2009).

[37] A. S. Grzegorzewski, M. Cialone, A. J. Lansen, M. van Ledden, J. Smith, T. Wamsley, The influence of barrier islands on hurricane-generated storm surge and waves in Louisiana and Mississippi, in: Proceedings from the 31st International Conference of Coastal Engineering, Hamburg, Germany, 2009 (2009).

[38] R. A. Luettich, J. J. Westerink, N. W. Scheffner, ADCIRC: An advanced three-dimensional circulation model for shelves coasts and estuaries, report 1: Theory and methodology of ADCIRC-2DDI and ADCIRC- 3DL, Tech. rep., United States Army Corps of Engineers (1992).

[39] J. J. Westerink, R. A. Luettich Jr, J. C. Feyen, J. H. Atkinson, C. N. Dawson, H. J. Roberts, M. D. Powell, J. P. Dunion, E. J. Kubatko, H. Pourtaheri, A Basin to Channel Scale Unstructured Grid Hurricane Storm Surge Model Applied to Southern Louisiana, Monthly Weather Review 136 (2008) 833–864 (2008).

[40] N. Booij, R. C. Ris, L. H. Holthuijsen, A third-generation wave model for coastal regions, Part I, Model description and validation, Journal of Geophysical Research 104 (1999) 7649–7666 (1999).

[41] M. Zijlema, Computation of wind-wave spectra in coastal waters with SWAN on unstructured grids, Coastal Engineering 57 (2010) 267–277 (2010).

[42] D. Roelvink, A. J. H. M. Reniers, A. van Dongeren, J. van Thiel de Vries, R. McCall, , J. Lescinski, Modelling storm impacts on beaches, dunes and barrier islands, Coastal Engineering 56 (2009) 1133–1152 (2009).

[43] J. L. Beven, H. Cobb, Tropical Cyclone Report, Hurricane Isabel, 6 - 19 September 2003, Tech. rep., National Hurricane Center (2003).

[44] U.S. Geological Survey, https://coastal.er.usgs.gov/hurricanes/isabel/, [Retrieved 20 July 2018] (2018).

[45] T. V. Wamsley, K. K. Hathaway, Monitoring morphology and currents at the Hatteras breach, Shore and Beach 72 (2004) 9–14 (2004).

[46] J. Hovis, W. Popovich, C. Zervas, J. Hubbard, H. H. Shih, P. Stone, Effects of hurricane isabel on water levels data report, April 2004, Tech. rep., National Oceanic and Atmospheric Administration (2004).

[47] J. M. Bonisteel, A. Nayegandhi, C. W. Wright, J. C. Brock, D. B. Nagle, Experimental advanced airborne research lidar (eaarl) data processing manual, Tech. Rep. 2009-1078, US Geological Survey (2009).

[48] A. H. Sallenger, C. W. Wright, K. Guy, K. Morgan, Assessing storm-induced damage and dune erosion using airborne Lidar: Examples from Hurricane Isabel, Shore and Beach 72 (2004) 25–29 (2004).

[49] U.S. Geological Survey, https://coastal.er.usgs.gov/data-release/doi-F76W9879/, [Retrieved November 2019] (2019).

[50] B. O. Blanton, S. Madry, K. Gallupi, K. Gamiel, H. Lander, M. Reed, L. Stillwell, M. Blanchard-Montogomery, R. Luettich, C. Mattocks, C. Fulcher, P. Vickery, J. Hanson, E. Devaliere, J. McCormick, Report for State of North Carolina Floodplain Mapping Project Coastal Flood Analysis System, Tech. Rep. TR-08-08, Renaissance Computing Institute (2008).

[51] H. Mitasova, M. F. Overton, J. J. Recalde, D. J. Bernstein, C. W. Freeman, Raster-based analysis of coastal terrain dynamics from multitemporal lidar data, Journal of Coastal Research 25 (2) (2009) 507—-514 (2009).

[52] H. Mitasova, L. Mitas, R. S. Harmon, Simultaneous spline approximation and topographic analysis for lidar elevation data in open-source gis, IEEE Geoscience and Remote Sensing Letters 2 (2005) 375–379 (2005).

[53] S. Bunya, J. C. Dietrich, J. J. Westerink, B. A. Ebersole, J. M. Smith, J. H. Atkinson, R. E. Jensen, D. T. Resio, R. A. Luettich, C. N. Dawson, V. J. Cardone, A. T. Cox, M. D. Powell, H. J. Westerink, H. J. Roberts, A high-resolution coupled riverine flow, tide, wind, wind wave and storm surge model for southern Louisiana and Mississippi: Part I – Model development and validation, Monthly Weather Review 138 (2010) 345–377 (2010).

[54] M. E. Hope, J. J. Westerink, A. B. Kennedy, P. C. Kerr, J. C. Dietrich, C. N. Dawson, C. J. Bender, J. M. Smith, R. E. Jensen, M. Zijlema, L. H. Holthuijsen, R. A. Luettich Jr, M. D. Powell, V. J. Cardone, A. T. Cox, H. Pourtaheri, H. J. Roberts, J. H. Atkinson, S. Tanaka, H. J. Westerink, L. G. Westerink, Hindcast and Validation of Hurricane Ike (2008) Waves, Forerunner, and Storm Surge, Journal of Geophysical Research: Oceans 118 (2013) 4424–4460 (2013).

[55] J. C. Dietrich, M. Zijlema, J. J. Westerink, L. H. Holthuijsen, C. N. Dawson, R. A. Luettich, R. E. Jensen, J. M. Smith, G. S. Stelling, G. W. Stone, Modeling hurricane waves and storm surge using integrally-coupled, scalable computations, Coastal Engineering 58 (2011) 45–65 (2011).

[56] K. M. Dresback, J. G. Fleming, B. O. Blanton, C. Kaiser, J. J. Gourley, E. M. Tromble, R. A. Luettich, R. L. Kolar, Y. Hong, S. Van Cooten, H. J. Vergara, Z. Flamig, H. M. Lander, K. E. Kelleher, K. L. Nemunaitis-Monroe, Skill assessment of a real-time forecast system utilizing a coupled hydrologic and coastal hydrodynamic model during Hurricane Irene (2011), Continental Shelf Research 71 (2013) 78–94 (2013).

[57] L. Schambach, A. R. Grilli, S. T. Grilli, M. R. Hashemi, J. W. King, Assessing the impact of extreme storms on barrier beaches along the atlantic coastline: Application to the southern rhode island coast, Coastal Engineering 133 (2018) 26–42 (2018).

[58] J. A. Roelvink, Coastal morphodynamic evolution techniques, Coastal Engineering 53 (2006) 277–287 (2006).

[59] C. M. Nederhoff, Modeling the effects of hard structures on dune erosion and overwash: Hindcasting the impact of hurricane sandy on new jersey with xbeach., Master's thesis, Delft University of Technology, Delft, ND. (2014).

[60] J. Sutherland, A. H. Peet, R. L. Soulsby, Evaluating the performance of morphological models, Coastal Engineering 51 (2004) 917–939 (2004).

[61] J. Bosboom, A. J. H. M. Reniers, A. P. Luijendijk, On the perception of morphodynamic model skill, Coastal Engineering 94 (2014) 112–125 (2014).

[62] D. Roelvink, A. J. H. M. Reniers, A. van Dongeren, J. van Thiel de Vries, J. Lescinski, R. McCall, Xbeach model description and manual, Tech. rep., UNESCO-IHE Institute for Water Education, Deltares and Delft University of Technology (2010).

Table 1: Settings for XBeach input parameters in this study.

Input Parameter	Typical Value(s)	This Study
Morphological acceleration factor, f_{mor}, `morfac`	1 to 10 [33, 32]	10
Maximum shields parameter, $\theta_{\max}$, `smax`	0.8 to 1.2 [33, 31]	0.8
Wave asymmetry and skewness, γ_{ua}, `facua`	0.1 to 0.3 [59, 57]	0.3
Critical avalanching slope under water, `wetslp`	0.1 to 1.0 [33, 62]	0.2
Threshold water depth to include Stokes drift, $h_{\min}$	0.001 to 1.0 [33, 62]	0.05

Table 2: Locations near NC where observations were collected during the study period. Significant wave heights were observed at four buoys operated by the NOAA National Data Buoy Center (NDBC) and at a directional waverider operated by the USACE Field Research Facility (FRF) in about 17 m depth offshore of Duck. Water levels were observed at four stations operated by the NOAA National Ocean Service (NOS).

Agency	ID	Name	Longitude	Latitude	Waves	Water Levels
NDBC	41001	East of Cape Hatteras	72.617 W	34.625 N	X	
NDBC	41002	South of Cape Hatteras	74.840 W	31.760 N	X	
NDBC	41025	Diamond Shoals	75.403 W	35.005 N	X	
NDBC	FPSN7	Frying Pan Shoals	77.590 W	33.485 N	X	
FRF	44056	Offshore of Duck	75.700 W	36.168 N	X	
NOS	8658120	Wilmington	77.953 W	34.227 N		X
NOS	8656483	Beaufort, Duke Marine Lab	76.670 W	34.720 N		X
NOS	8652587	Oregon Inlet Marina	75.548 W	35.795 N		X
NOS	8651370	Duck	75.747 W	36.183 N		X

Table 3: Total Volume (10^5 m^3) of erosion and deposition for each section on 30-km domain compared to observation. The area of computation is limited to each section and the extent of available LiDAR data

	Prediction		Observation		Area (10^3 m^2)
Section	Erosion	Deposition	Erosion	Deposition	
North	1.36	0.51	1.45	0.70	320.6
Middle	1.11	0.43	1.21	0.53	309.5
South	0.89	0.39	0.95	0.46	301.7

Table 4: Details of mesh resolution and model performance for the sensitivity tests on the 4-km mesh.

	Spacing (m)		Performance					
			On Mesh			On Raster		
Mesh	Alongshore	Cross-shore	SS_1	B_{MN_1}	N_1	SS_2	B_{MN_2}	N_2
Base	15	3	0.68	-0.06	15423	0.68	-0.06	641893
C5	15	5	0.6	-0.05	9260	0.58	-0.06	641893
C10	15	10	0.51	-0.03	4620	0.34	-0.04	641893
C15	15	15	0.27	-0.03	3086	0.21	-0.03	641893
C30	15	30	0.07	0.334	1521	-0.03	0.2	641893
L5	5	3	0.68	-0.06	46299	0.72	-0.07	641893
L10	10	3	0.69	-0.07	23134	0.7	-0.07	641893
Base	15	3	0.68	-0.06	15423	0.68	-0.06	641893
L20	20	3	0.69	-0.06	11556	0.68	-0.06	641893
L30	30	3	0.69	-0.06	7706	0.65	-0.05	641893
L50	50	3	0.67	-0.05	4603	0.6	-0.05	641893
L100	100	3	0.69	-0.03	2279	0.53	-0.02	641893
L200	200	3	0.69	-0.03	1159	0.44	-0.02	641893

Table 5: Optimum "wetslp" value and model accuracy for each mesh

				On Mesh		On Raster	
Mesh	Alongshore	Cross-shore	*wetslp*	SS_1	B_{MN_1}	SS_2	B_{MN_2}
Base	15	3	0.2	0.68	-0.06	0.68	-0.05
C5	15	5	0.15	0.71	-0.04	0.68	-0.05
C10	15	10	0.1	0.79	0.02	0.64	-0.03
C15	15	15	0.1	0.73	-0.02	0.48	0.04
C30	15	30	0.05	0.92	0.01	0.25	-0.05

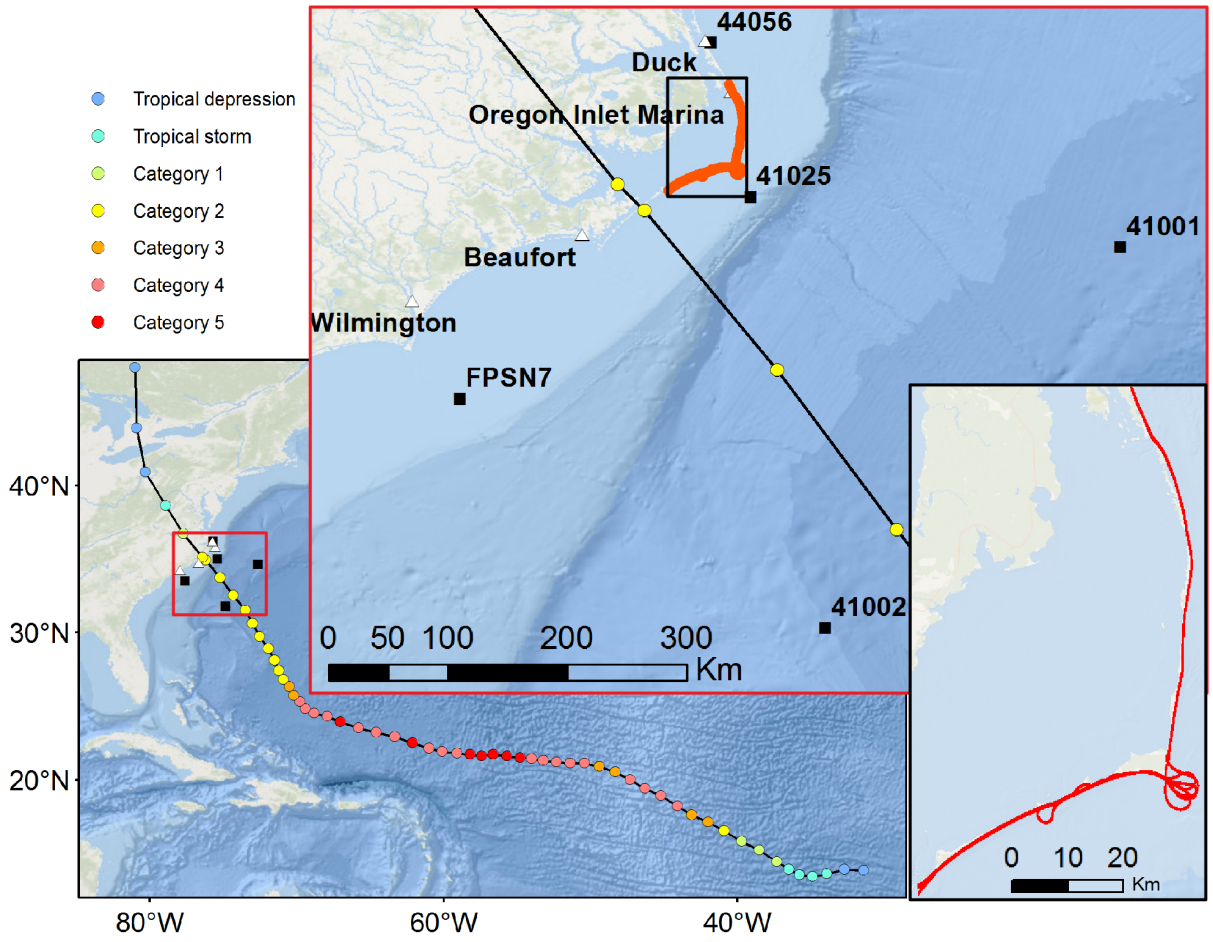

Figure 1: Hurricane Isabel (2003) track (colors show the storm intensity), with successive insets to show coastal NC and Hatteras Island. The extents of available pre- and post-storm LiDAR surveys (red line), and the locations of wave buoys (black squares) and water level stations (white triangles) are also shown.

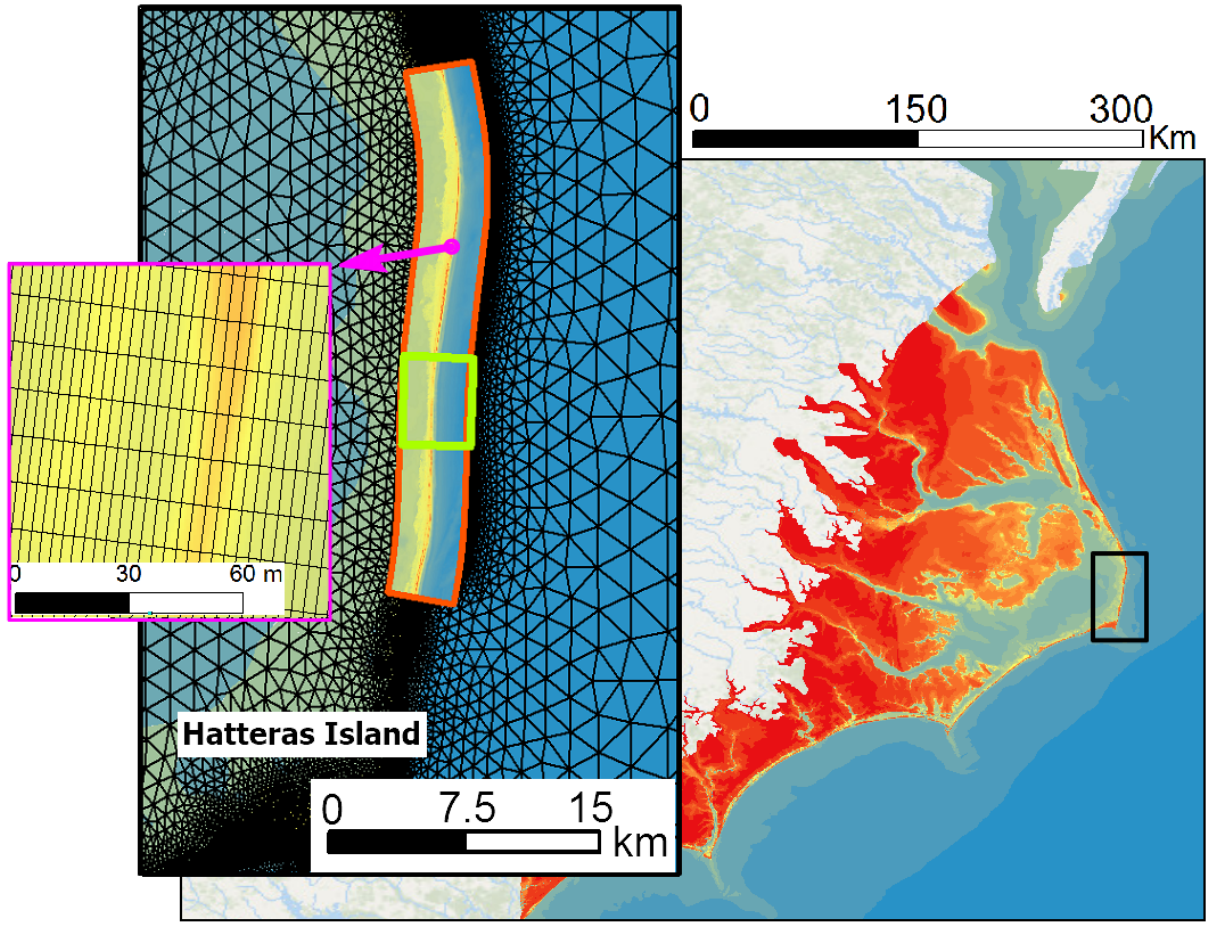

Figure 2: Comparison of meshes for ADCIRC+SWAN and XBeach. The region-scale ADCIRC+SWAN mesh is shown with contoured bathymetry/topography (right) and as black triangular elements in the first inset (center). The 30-km (red box) and 4-km (green box) extents of the XBeach mesh are shown in the first inset (center), with a maximum resolution shown in the second inset (left).

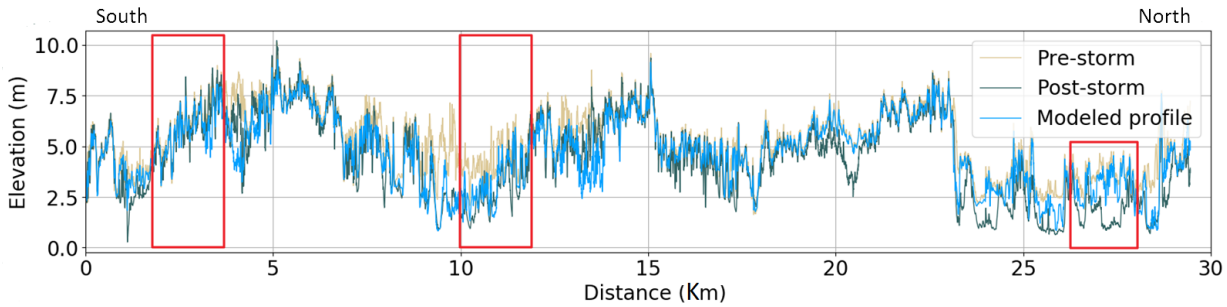

Figure 3: Observed and predicted dune crest profiles along the 30-km study area, for alongshore distances starting from north of Avon and ranging from south to north. The largest dune elevation change of about 4 m occurs near town of Salvo (at an alongshore distance of about 10 km), and the lowest dunes and extensive overwash were located near Rodanthe (at an alongshore distance of about 25 km). The red boxes correspond to the location of the three regions specified in Figure 7.

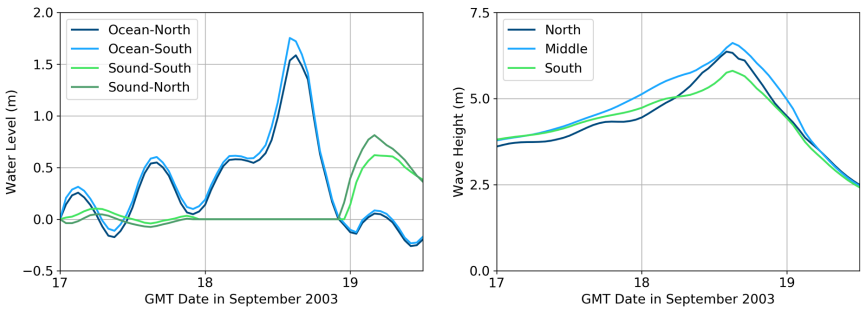

Figure 4: Boundary conditions extracted from ADCIRC+SWAN and used in XBeach. The water levels are interpolated from ADCIRC to the four corners of the XBeach mesh; the left sub-figure shows the time series used for the 30-km XBeach mesh. During the peak of the storm, water levels are set to zero at the sound-side boundary to maintain a positive water depth in XBeach. The wave parameters (significant height, peak period, mean direction) are interpolated from SWAN at 15 points along the offshore boundary; the right sub-figure shows the time series for significant wave heights at three locations in the 30-km XBeach mesh.

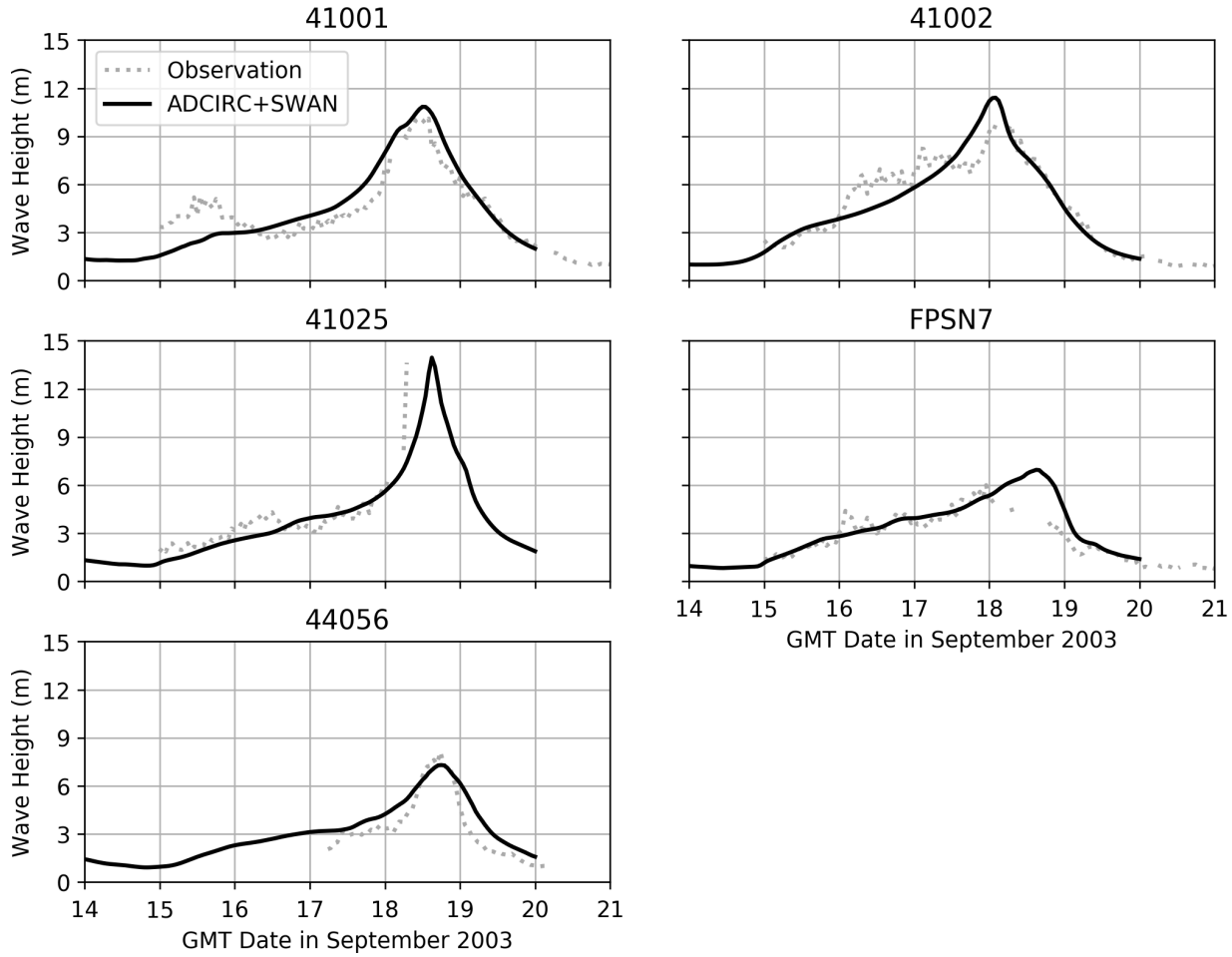

Figure 5: Time series of observed and predicted significant wave heights (m) from simulations at 5 stations with locations described in Table 2 and Figure 1.

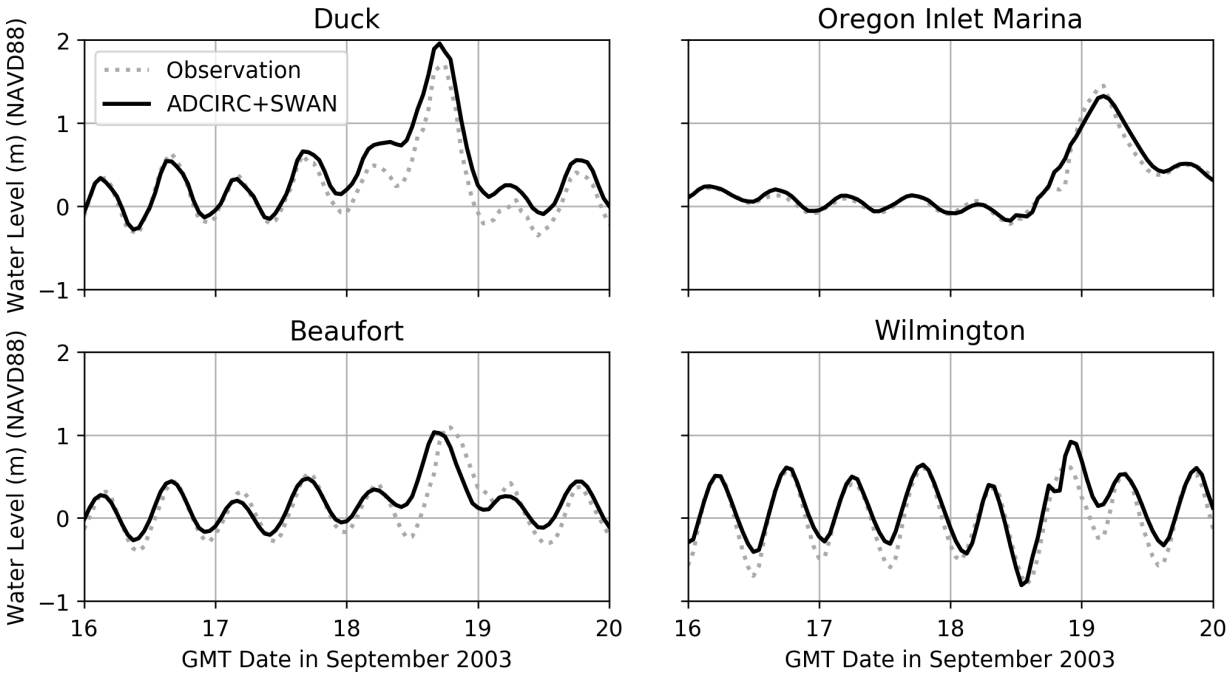

Figure 6: Time series of observed and predicted water levels (m) (NAVD88) from simulations at 4 stations with locations described in Table 2 and Figure 1.

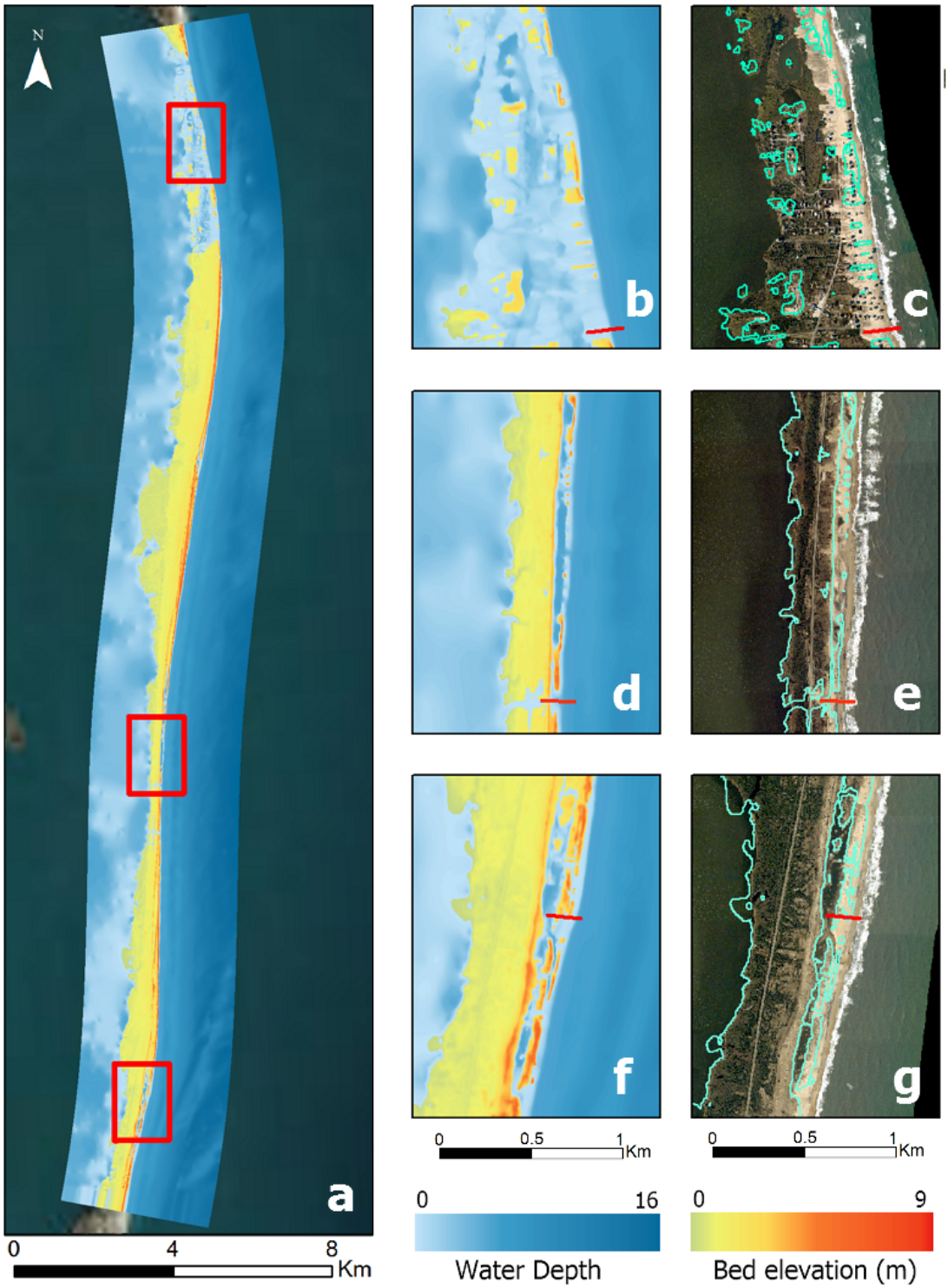

Figure 7: XBeach-predicted peak water levels on the (left column) full, 30-km domain and (middle) at selected locations, with comparisons to (right) aerial photos. In the aerial photos, the XBeach-predicted flooding extents are shown in a cyan line, and match well with the observed overwash fans. The red lines in panels b, d and f show the location of beach profiles in Figures 9 and 16.

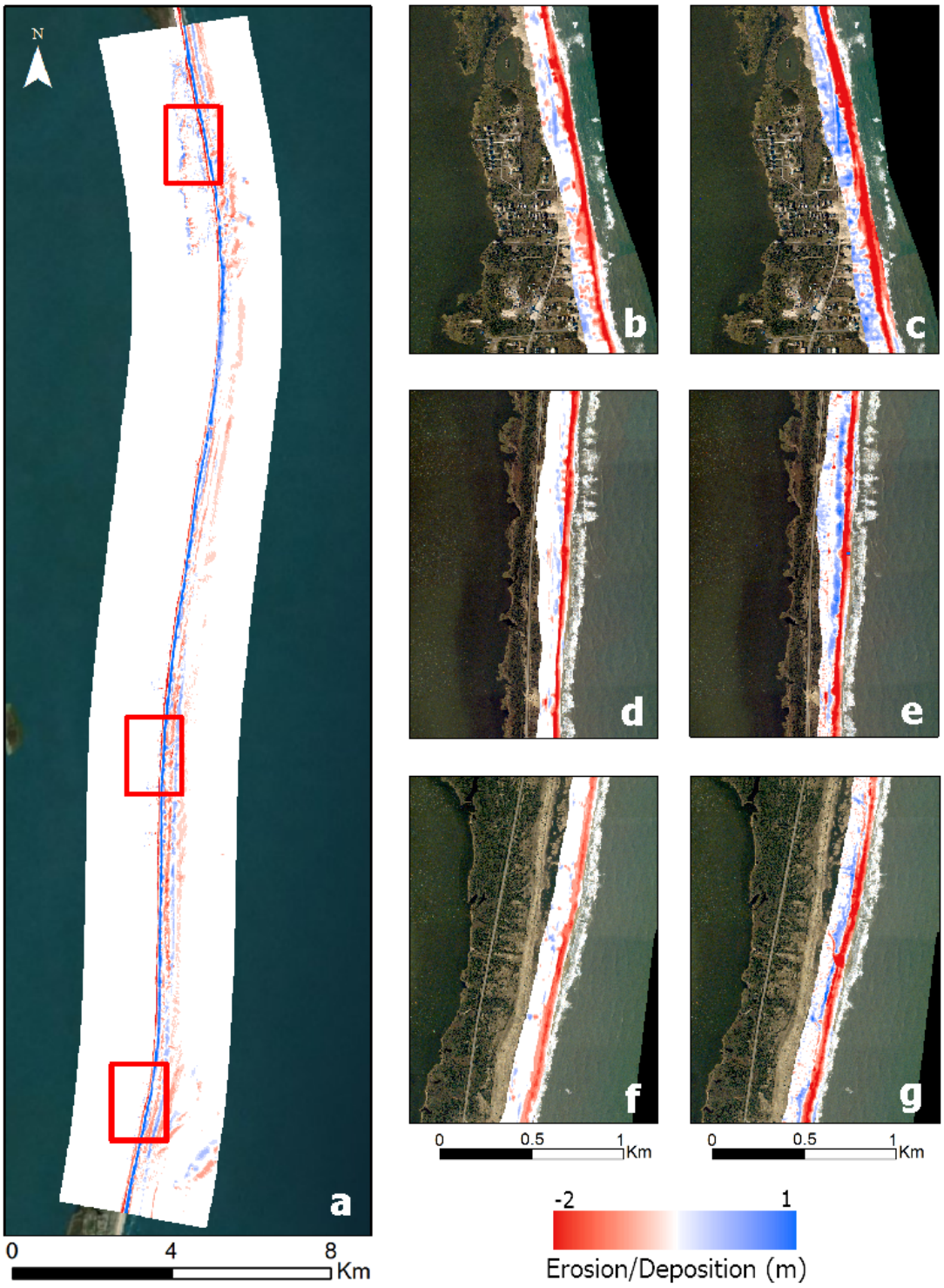

Figure 8: Erosion and deposition predicted by XBeach on the entire computational domain (left). XBeach prediction at the selected locations and only to the extent of available LiDAR data (middle) with comparison to observed erosion and deposition (right) extracted from LiDAR. Red and blue colors indicate erosion and deposition, respectively.

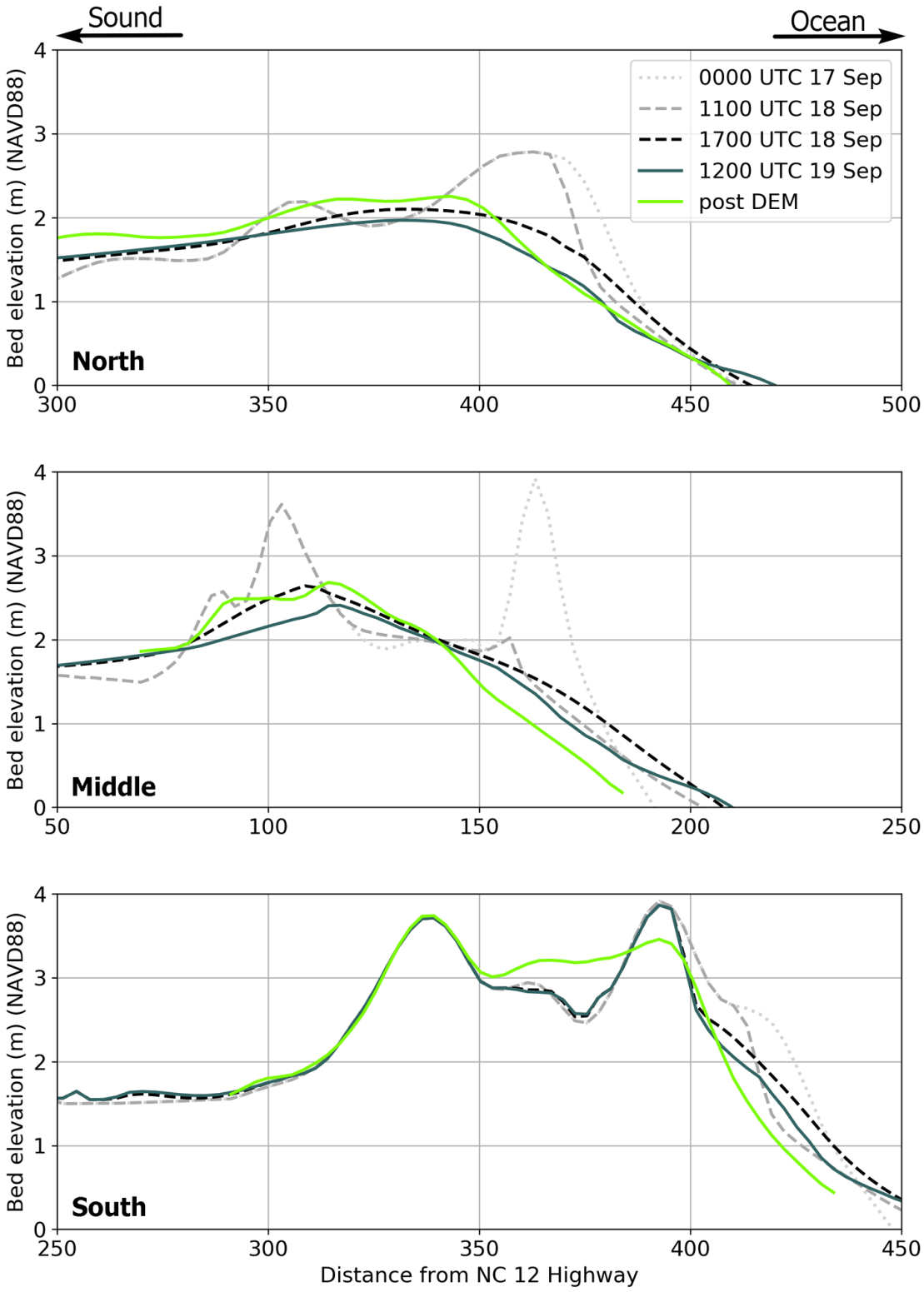

Figure 9: Beach profile at different time steps compared to the LiDAR post-storm profile at the locations specified in Figure 7.

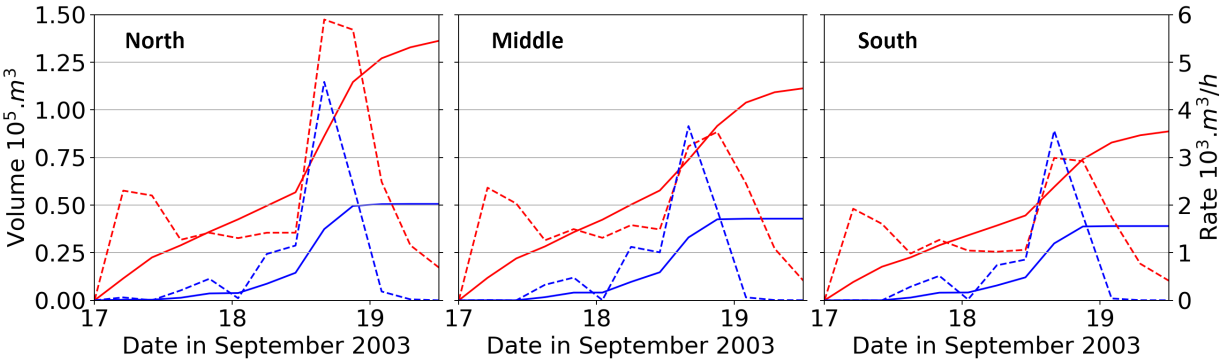

Figure 10: Volume (solid) and rate (dashed) of erosion (red) and deposition (blue) on 30-km domain.

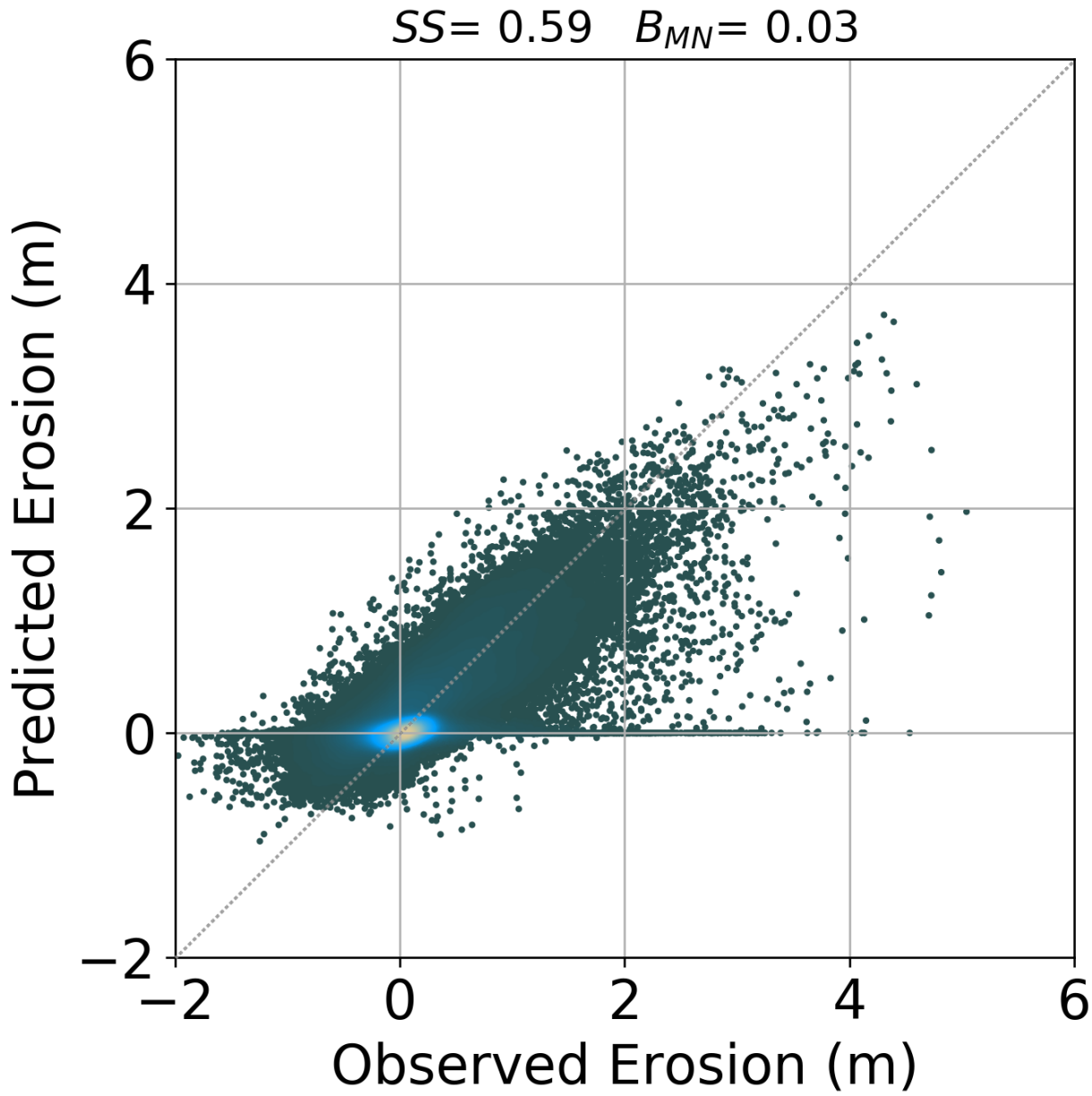

Figure 11: Scatter plot comparing observed and predicted elevation changes for the XBeach simulation on the 30-km domain.

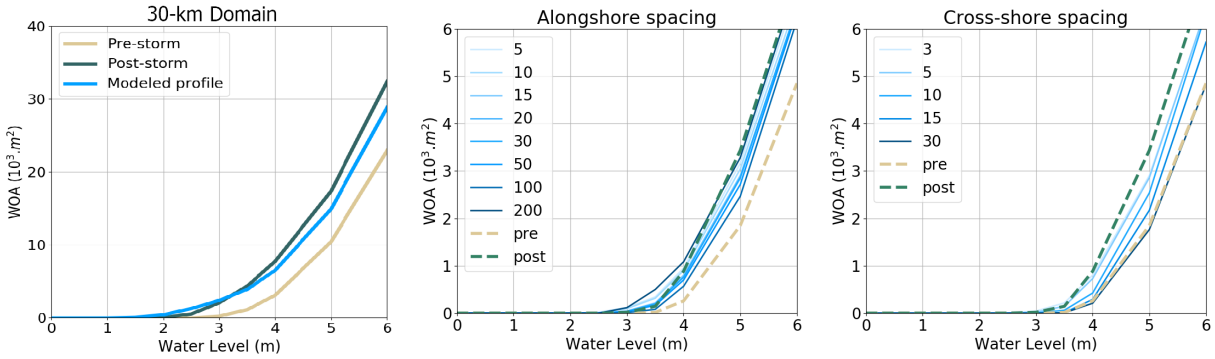

Figure 12: Water Overpassing Area (WOA) for the 30-km domain (left) and for meshes with varying spacing in alongshore (middle) and cross-shore (right) directions.

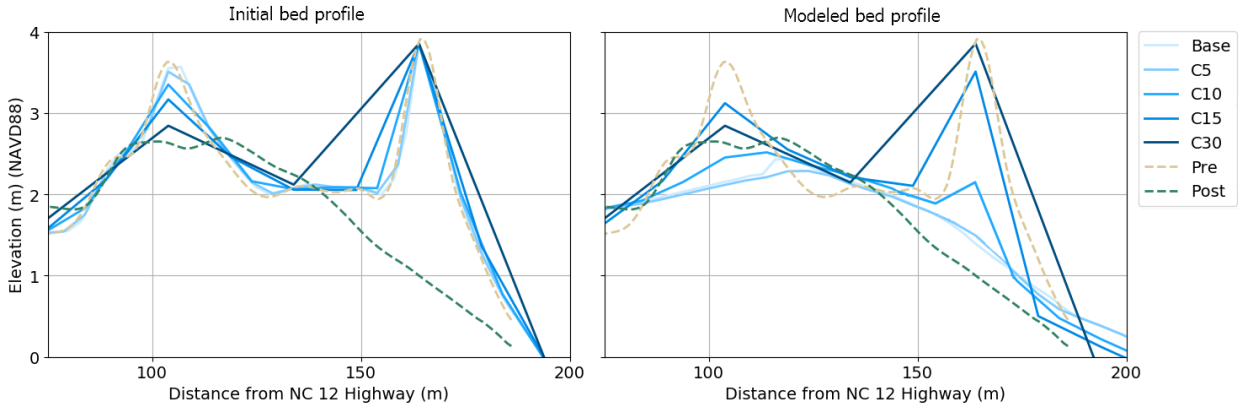

Figure 13: Effect of mesh resolution on predicted topographic elevations at the Middle profile with location shown in Figure 7e.

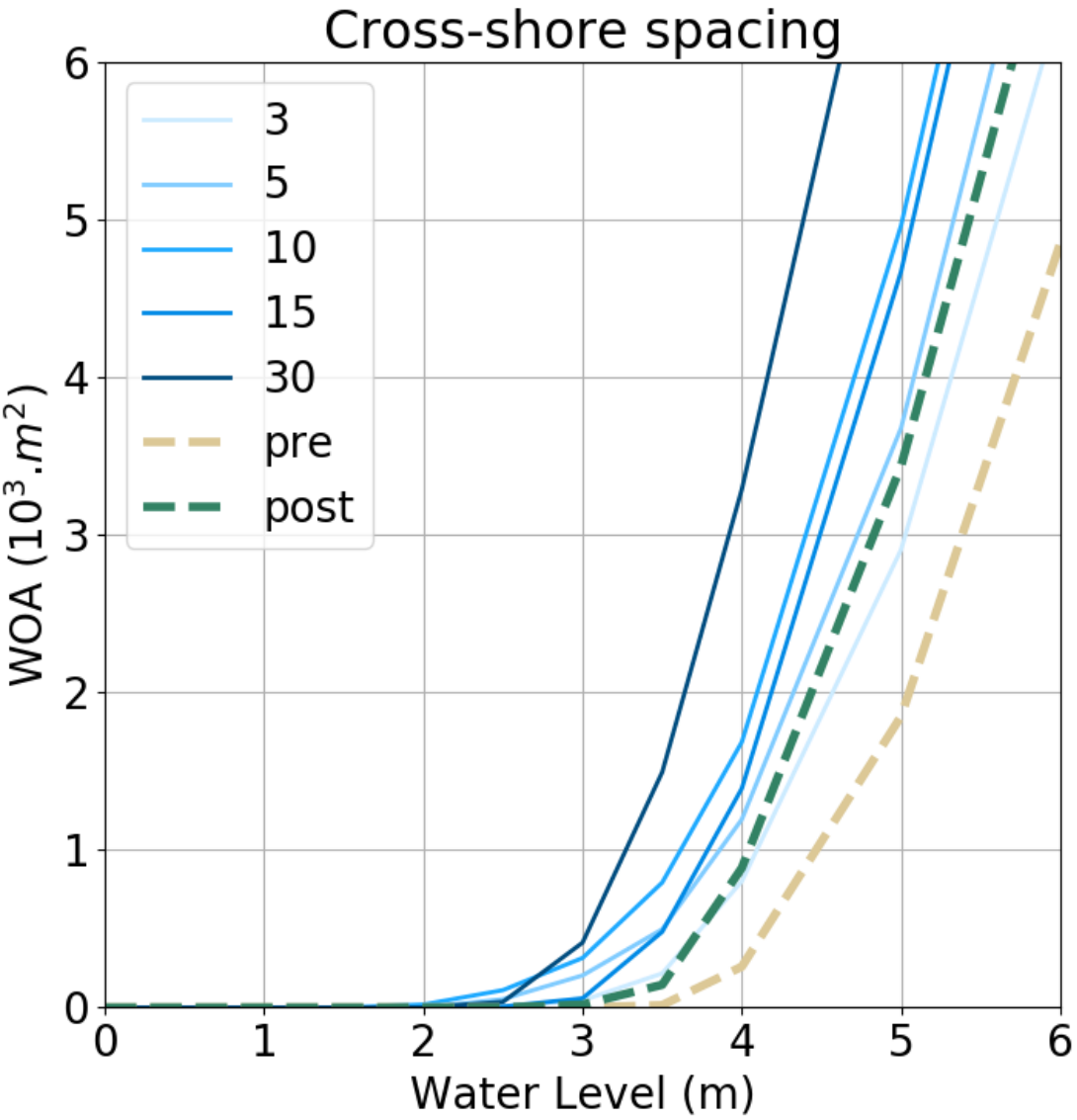

Figure 14: Water Overpassing Area (WOA) for meshes with varying spacing in cross-shore directions and with different *wetslp* – refer to Table 5

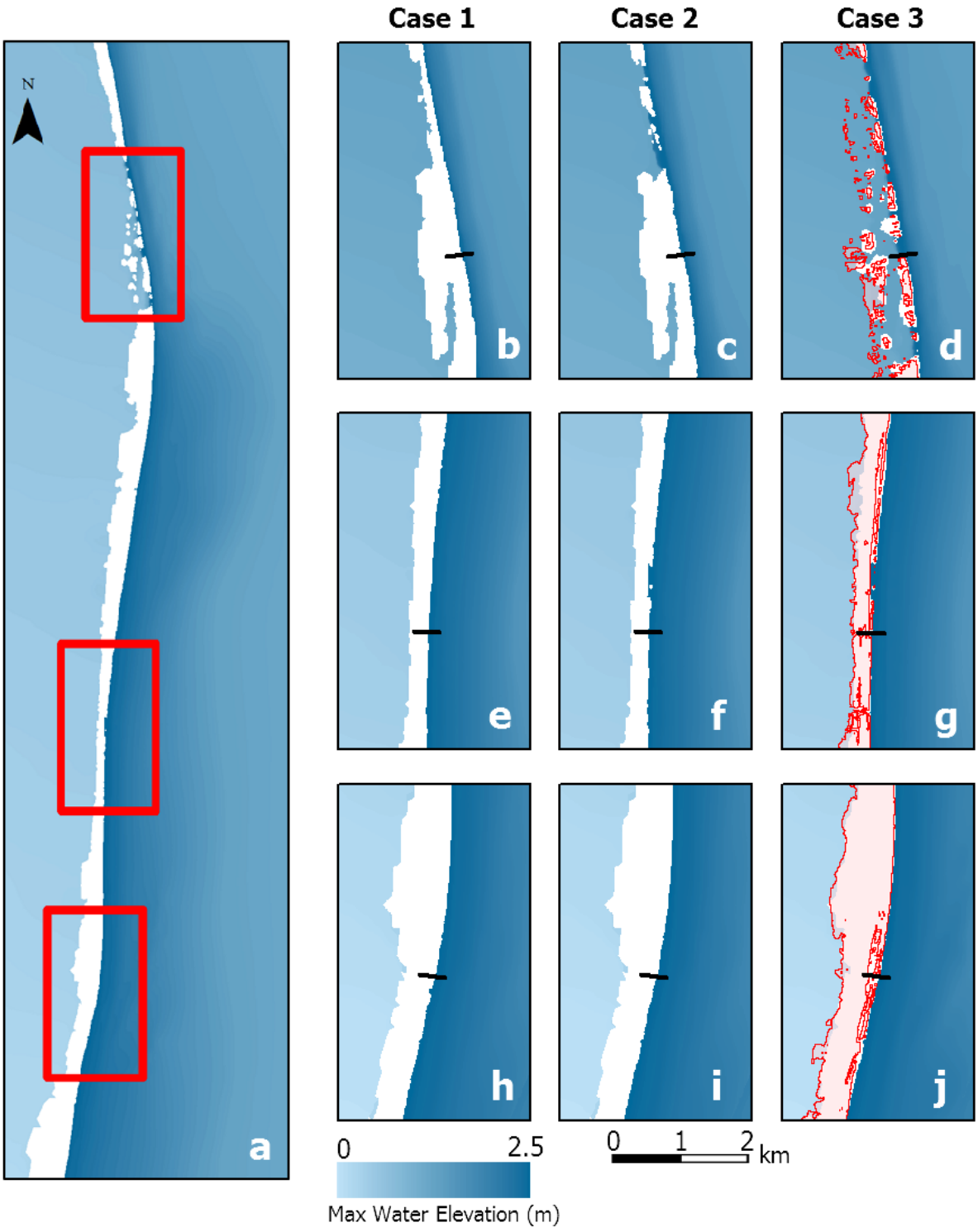

Figure 15: Maximum water levels from ADCIRC+SWAN for Cases: (1) pre-storm topography (b, e, h), (2) post-storm topography (c, f, i), and (3) XBeach predicted topography (d, g, j). The top, middle and bottom row correspond to the red boxes. In the last column, the red lines show the extents of the XBeach-predicted maximum flooding, and the black lines show the locations of profile transects in Figure 16.

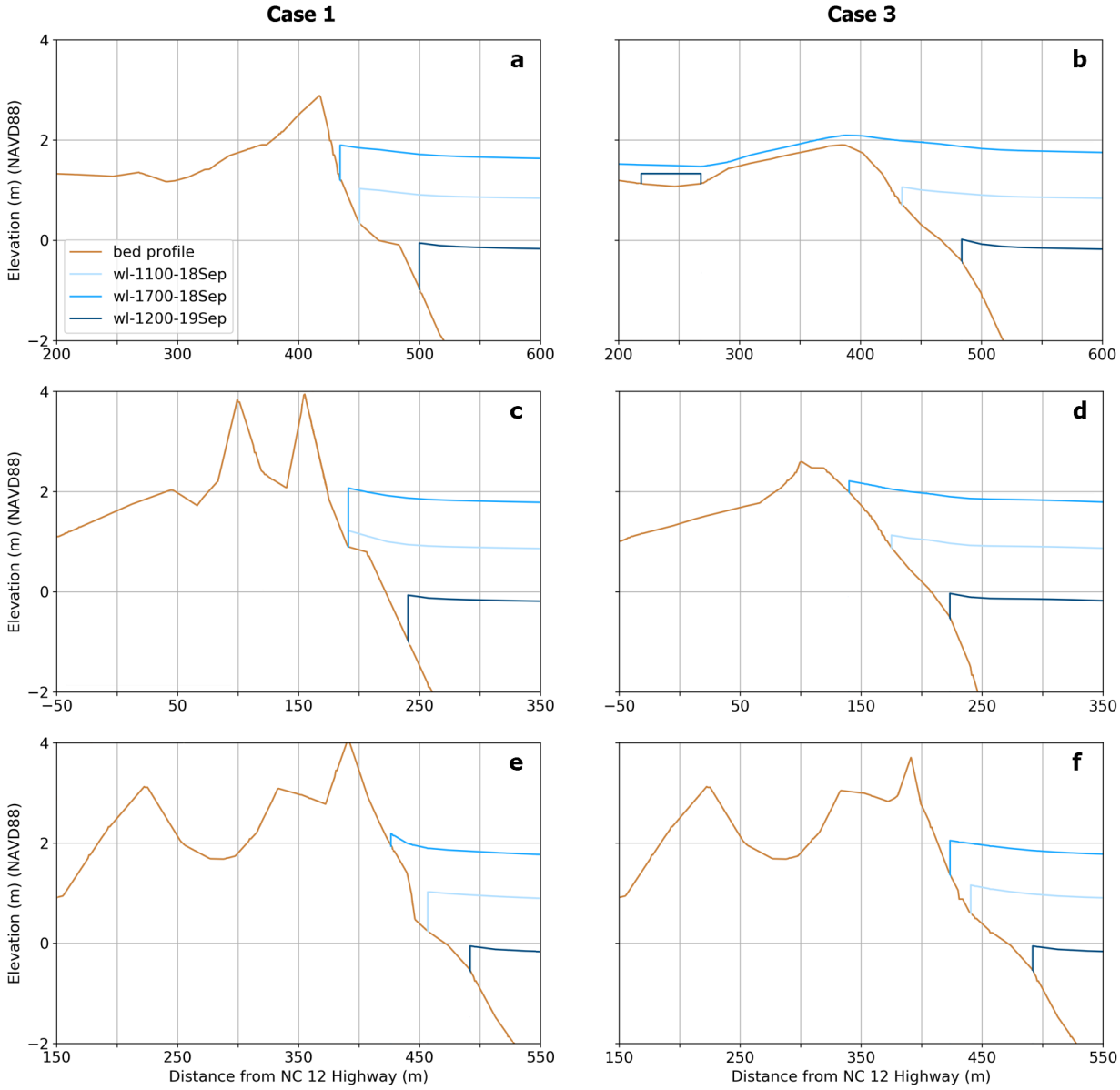

Figure 16: bed profile and predicted water levels in Case 1 (left column) and Case 3 (right column) at sections shown in Figure 15. Sub-figures at top, middle and bottom correspond to the north, middle and south sections.

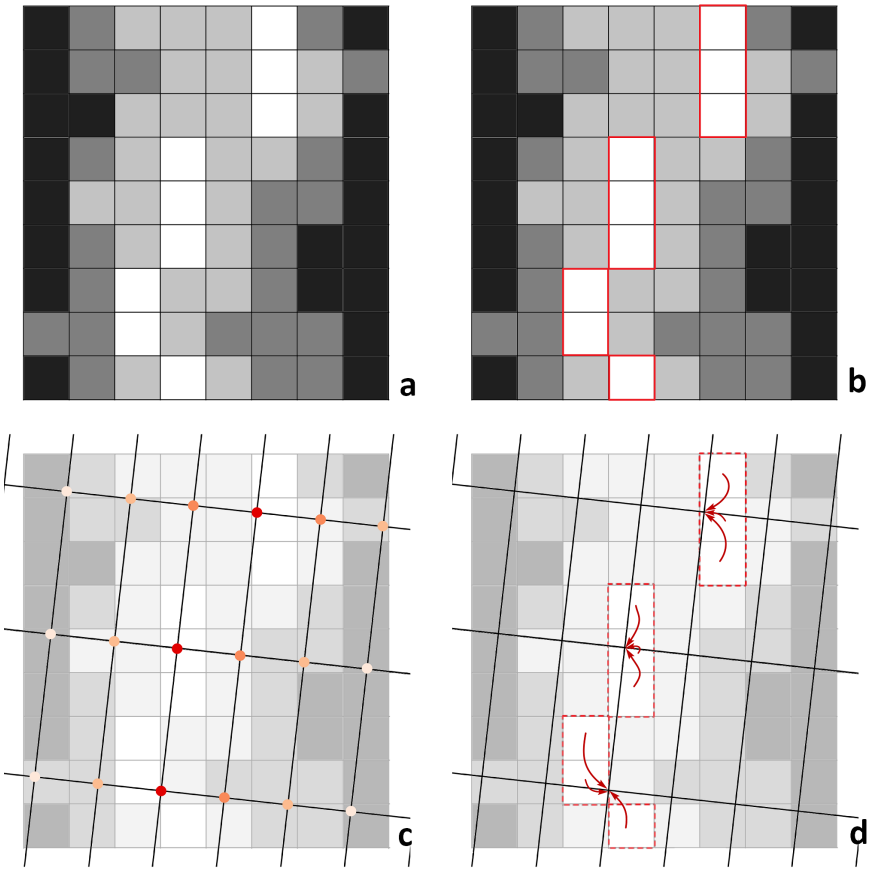

Figure 17: Schematic representation of the post-processing steps toward correcting the dune crest elevation: (a) the DEM, (b) finding the highest points (dune crest) on the DEM, (c) finding the highest cells in the XBeach mesh, and (d) assigning the average of the nearest highest points from the DEM onto the XBeach mesh.